

本資料は 年 月 日付けで登録区分、  
変更する。

2001. 7. 31

[技術情報室]

分 置

# Neutron and Gamma-Ray Streaming Experiments at the Fast Neutron Source Reactor "YAYOI" \*

July, 1979

本資料の全部または一部を複写・複製・転載する場合は、下記にお問い合わせください。

〒319-1184 茨城県那珂郡東海村大字村松4番地49  
核燃料サイクル開発機構  
技術展開部 技術協力課

Inquiries about copyright and reproduction should be addressed to:  
Technical Cooperation Section,  
Technology Management Division,  
Japan Nuclear Cycle Development Institute  
4-49 Muramatsu, Tokai-mura, Naka-gun, Ibaraki, 319-1184  
Japan

© 核燃料サイクル開発機構 (Japan Nuclear Cycle Development Institute)



Neutron and Gamma Ray Streaming Experiments  
at the Fast Neutron Source Reactor "YAYOI"\*

Yoshiaki Oka,\*\* Ichiro Yanagisawa\*\*  
Masatsugu Akiyama,\*\* Shigehiro An\*\*

A b s t r a c t

Neutron and gamma ray streaming experiments were performed in the ducts and cavities that were located in the heavy concrete shields of the fast neutron source reactor YAYOI of University of Tokyo. The configurations have the feature that the streaming through the ducts are occurred following the scattering in the cavity. The axes of the ducts are perpendicular to the source radiation from the core. The spectrum of the source was modified by putting a plug in the beam hole of the core. An aluminum plug and the plug which contains paraffin were used. The decay in the ducts, however, hardly depends on the source spectrum. The decay in the ducts is nearly exponential.

---

\* Work performed by University of Tokyo, under contract with Power Reactor and Nuclear Fuel Development Corp.

\*\* Nuclear Engineering Research Laboratory, the Faculty of Engineering, the University of Tokyo

## CONTENTS

	Page
1. Purpose .....	1
2. Experimental Configuration .....	2
3. Measuring Instruments .....	4
4. Experimental Results .....	8
4-1 Measurement results in cavity by TLD .....	8
4-2 Measurement results in cavities by BF counter .....	11
4-3 Foil reaction rate distribution in cavity ....	12
4-4 Measurement results by BF counter, of duct streaming .....	13
4-5 Measurement results by TLD, of duct streaming .....	16
5. Summary of Experimental Results and its Consideration .....	18
6. Conclusion .....	20
7. Figures and Tables .....	21

## 1. Purpose

It poses often a problem for the study of actual shield design to know what distribution will be presented by neutron and gamma-ray when they leak into broad space (cavity) through penetrated portions on shielding body and further to know the degree of leakage into the space through ducts leading to the cavity. For example, in case of a sodium cooled fast reactor, radiation to pump rooms by the neutron streaming through sodium coolant piping and the radiation leakage into other surrounding rooms, etc. should be taken into account. The data available for such streamings as those occurring through cavity are very few in number, however, and it may be said that calculation code effectiveness on the above stated conditions is not checked completely in reference to experiments.

The heavy concrete shield of the fast neutron source reactor "YAYOI" of University of Tokyo has two cavities called fast column and thermal column (moderator not included), to which various ducts are fitted. These cavities are suitable for obtaining fundamental data of such systems structure. In this study, therefore, the streaming experiment of cavity system by "YAYOI" has been performed, for the purpose of acquir-

ing fundamental data on radiation streaming comparable with calculation results.

## 2. Experimental Configuration

Putting the reactor core on the operating position of "YAYOI" B, experimental holes of 20 cm $\phi$  approx. were prepared through the two cavities facing with each other on horizontal center line of the core, to let neutron and gamma-ray leak from the reactor core.

The experimental system and the reactor core structure of "YAYOI" are shown in Fig. 2-1 and Fig. 2-2, respectively.

The core of "YAYOI" is a horizontal column formed by 93% enriched metallic uranium having the dimension of 125 mm $\phi$  x 150 mm approx. The core is covered with a blanket of 0.4% depleted uranium, and two lead reflectors A and B are fitted on the blanket.

The two cavities of "YAYOI" are located on horizontal center line of the core. The one on left side from the reactor front face and the other on right side are called fast column cavity and thermal column cavity, respectively. At the fast column side, neutron and gamma-ray emitted from the reactor core leak into the cavity through the reflector beam hole from

the blanket surface, while at the thermal column side, they penetrate into the cavity through the beam hole leading nearly to core fuel within the blanket.

10 cm $\phi$  beam hole at the reflector A becomes 20 cm $\phi$  at the reflector B (lead) fixed to the system structure, being further connected to 20 cm $\phi$  beam hole in the heavy concrete board (36 cm T) fitted to the outside of the structure. The heavy concrete forms one face of the cavity wall. The two cavities are almost symmetry through the core center and have the dimensions of 1.5 mW x 1.5 mH x 1.63 mD. Beam leakage on the thermal column takes place through the blanket, which causes spectrum to appear somewhat hard and stiff. Gamma dose distribution and neutron reaction rate distribution in the both cavities were measured. Caving wall is surrounded by heavy concrete whose internal face is coated with 5 mm steel plate.

Experimental holes of various sizes are led to these cavities. The streaming of neutron and gamma-ray was measured in the following ducts: the thermal column upper portion ducts No. 23, No. 25, No. 27 (two-stepped ducts of 10 cm $\phi$  x 80 cm L and 20 cm $\phi$  x 70 cm L) and No. 31 (10 cm $\phi$  x 150 cm L), and a two-stepped big duct No. 26 (30 cm $\phi$  x 80 cm L and 46 cm $\phi$  x 70 cm L) on the fast column side. These ducts are

not located at the points from where direct observation of radiation source is available. Neutron and gamma-ray once scattered in cavity are regarded as radiation source of streaming. This shows the characteristics of the experimental system structure concerned. In case where no plug is inserted into beam hole, the incident beam contains many fast neutrons. In order to survey radiation streaming in the ducts when incident beam spectrum is softened, measurements were also conducted for such a case as aluminum plug of 32 cm T x 20 cm $\phi$ , and plug of lead (12 cm) + graphite (15 cm) + paraffin (9 cm) are inserted into beam holes on the heavy concrete board, that is, data were taken for the following cases.

- A) Without plug
- B) Aluminum plug
- C) Lead + Graphite + Paraffin Plug. This is to be called henceforth as paraffin-contained plug.

### 3. Measuring Instruments

$\mu\text{BF}_3$  counter,  $^6\text{LiF}$  TLD, gold foil and indium foil were used for neutron measurement; and for gamma-ray,  $\text{CaSO}_4$  TLD was employed.

(1)  $\mu\text{BF}_3$  counter

Mitsubishi Electric Machinery Co.'s  $\mu\text{BF}_3$  counter of 6 mm $\phi$  approx. (ND-8512-90) was in use. Detector moving apparatus was set on the top of the reactor shield, and  $\mu\text{BF}_3$  counter was fixed, together with cable, to the end of aluminum pipe passed through by a string which was being perpendicularly stretched. And the measurement was performed moving gradually the counter by a certain distance upward or downward by means of the detector moving apparatus. At this time, pre-amplifier, high-voltage wire and scaler timer were being fixed to the top of the reactor shield. In addition, the measurement was also carried out in case where 2 mm thick cylindrical cadmium cover is fitted to  $\mu\text{BF}_3$  counter. By using the detector moving apparatus, the very accurate measurement became possible. Due to the elongation of string used, however, the slight error was observed in the measuring positions.

(2) TLD

$^6\text{LiF}$  TLD (Matsushita Denki UD 136N),  $^7\text{LiF}$  TLD (UD 137N) and  $\text{CaSO}_4$  TLD (UD 110S) were employed. UD-502A of Matsushita Denki was adopted

as TLD reader, and reader calibration was conducted by  $^{60}\text{Co}$  standard Source. The simultaneous irradiation was performed by sticking these TLDs to the string stretched.

Subtracting emission rate of UD 137N from that of UD 136N, emission rate of  $^{60}\text{Co}$  gamma-ray equivalence by neutron reaction was figured out. The subtracted rate was under 10% because of the immense emission rate of UD 136N.

Gamma-ray dose calculated from emission rate of  $\text{CaSO}_4$  TLD and was shown in R/h unit. Strictly speaking, as absorption coefficient of  $\text{CaSO}_4$  is not equal to that of air, Rentogen representation is not correct. But as it is often adopted, this representation was offered for convenience' sake. The value obtained from  $^7\text{LiF}$  TLD emission rate was nearly coincident with that from  $\text{CaSO}_4$  within error range.  $^7\text{Li}$  threshold reaction contribution due to fast neutron is considered to be not so large even at points nearby the reactor core.

The measurement results were presented in converted values calculated for the case where every item was irradiated by 2 KW for one hour. As the measuring points were on the string, the

measurement data could be obtained not only on the ducts axes but also at the horizontal points in the cavities without ducts.

(3) Gold foils

Cylindrical gold foils of 0.05 mmT x 6 mm $\phi$  approx., which were stuck to tapes on the string, were irradiated. Gold foils covered with cadmium sheet of 1 mmT were also in use. 412 keV gamma-ray of  $^{198}\text{Au}$  produced through  $^{197}\text{Au}$  (n,  $\gamma$ ) reaction after irradiation was measured with Ge (Li) semi-conductor detector, and reaction rate was obtained from photo-peak count. The foils directions were perpendicular to the axes of beams leaking horizontally from the reactor core.

(4) Indium foils

Indium foils of 0.5 mm T x 12.4 mm $\phi$  was employed to detect fast neutron at the outlet of beam hole. The foils were first enveloped in cadmium cover of 1 mm T for irradiation. 335 KeV gamma-ray of  $^{115\text{m}}\text{In}$  produced through  $^{115}\text{In}$  (n, n $''$ ) reaction was measured by the same process as in the case of gold foils in order to know the reaction rate.

#### 4. Experimental Results

##### 4-1 Measurement results in cavity by TLD

First of all, the measurement results in thermal column cavity by means of TLD is described. Fig. 4-1 shows TLD measuring position of the thermal column. The measuring points were taken along the dotted-lines in the Fig. 4-1. Upwards distance from the surface of the heavy concrete-made platform car, cavity floor, is represented by  $H$ , depth distance from the heavy concrete board is shown by  $D$  and the horizontal distance from the heavy concrete wall side that intersects rectangularly with these two distances is shown by  $L$ . The point at  $H=75$  cm,  $D=0$  cm and  $L=75$  cm is the center of beam inlet to the cavity. Section A-A' in Fig. 4-1 shows the plane including beam axis parallel to the direction of beam injection into the cavity. And section B-B' indicates the plane rectangularly intersecting with it at the point of  $D=87.5$  cm.

The results by TLD of reaction rate distribution in the thermal column at the Section A-A' ( $L=75$  cm) are shown in Fig. 4-2, Fig. 4-3 and Fig. 4-4. These are in the cases with aluminum plug, paraffin contained plug and without beam hole plug, respectively. Height  $H=150$  cm is the dimension measured along the

opening wall of cavity ceiling duct at the face of A-A'. In this case, however, swelling in neutron reaction rate is perceived at the duct inlet. There is no swelling in gamma-ray. It is observed further that low reaction rate is perceivable at the both wall sides. Neutron reaction rate dampings towards depth on lines H=75 cm (on beam shaft), H=100 cm and H=125 cm on A-A' section face are shown in Fig. 4-5 and Fig. 4-6, in case with paraffin-contained plug and without plug, respectively. Although the damping on beam axis is very steep, swelling due reflection is perceived on the wall side of D=163 cm. In case of paraffin-contained plug, this swelling is not perceived and damping is not so deep as the above, being somewhat gradual.

Fig. 4-7, Fig. 4-8 and Fig. 4-9 show gamma-ray dampings at the same points as stated above, as to the cases "Without plug", "Aluminum plug" and "Paraffin-contained plug", respectively. Gamma-ray damping is more gradual than those of neutron shown in Fig. 4-5 and 4-6. Next, the measurement results obtained on line L=75 cm and line H=75 cm of section B-B' (D=87.5 cm) are shown in Fig. 4-10 ("Without plug") and Fig. 4-11 ("Paraffin-contained plug"), respectively. The lower figure shows the measurement results on the vertical line of L=75 cm, and the lower figure indicates

those on the horizontal line of  $H=75$  cm intersecting the vertical line rectangularly. From these figures it is evident that  $D=87.5$  cm face is almost on the middle point between cavity beam inlet and the confronting wall, the distribution of measurement results are almost symmetry as to right, left, lower and upper directions and that values nearby the walls drop a little.

Above described are the measurement results of thermal column cavities by TLD. The results about fast column cavities are given as follows. These results were obtained on lines of heights  $H=75$  cm (on beam axis),  $H = 100$  cm, and  $H = 125$  cm and  $H=150$  cm (nearby ceiling wall) at section A-A' including beam axis. The reaction rate distribution of TLD in use for neutron is presented in Fig. 4-12, Fig. 4-13 and Fig. 4-14 as to the cases "Without plug", "Aluminum plug" and "Paraffin-contained plug", respectively. The distribution tendency is similar to the case of thermal columns. The measurement value ( $H=150$  cm) nearly the wall of  $D=62.5$  cm, to which 30 cm square No. 26 duct is opened, is apparently a little lowered. This is presumably due to the fact that the big sectional area of No. 26 duct diminished wall scattering influence. Fig. 4-15, Fig. 4-16 and Fig. 4-17

present the measurement results of TLD in use for gamma-ray. As expected, influence by No. 26 duct on each measurement conducted for ceiling wall side portion (H=150 cm) was observed, irrespectively of plug type.

#### 4-2 Measurement results in cavities by $\mu\text{BF}_3$ counter

The results of measurement conducted by  $\mu\text{BF}_3$  counter on axes of ducts No. 23, No. 25, No. 27 and No. 31 (D=22.5, 62.5, 112.5 and 151.5 cm, respectively) at sectional face of A-A' within cavities are described underneath. No. of counts/W distribution of  $\mu\text{BF}_3$  counter in case of "Without plug", "Aluminum plug", and "Paraffin-contained plug" are presented respectively in Fig. 4-18, Fig. 4-19 and Fig. 4-20. The upper figure shows the results in case where cadmium cover is fitted and the lower figure indicates those in case without the cover. In any case, it is obvious that the distribution gets flatter as the distance from beam inlet increases. Furthermore, the distribution for "Paraffin-contained plug" is flatter as compared with that for "Without plug".

In case of "Without plug", value on D=151.5 cm axis nearby the wall around H=75 cm is larger than that on D=112.5 cm axis. This indicates that the

reflection influence from the wall is large. On the other hand, this does not apply for the cases of "Aluminum plug" and "Paraffin-contained plug".

In case where cadmium cover is fitted and "Without plug", the distribution at  $D=22.5$  becomes sharp, while in case "Paraffin-contained plug" the distribution gets steeper when the cover is not employed.

Small peaks are observed around duct inlet, irrespectively of plug type. This conforms to the fact that in TLD measurement neutron reaction rate around ducts is more raised compared with those in the surroundings.

Fig. 4-21 shows 3-dimensional representation of the distribution in thermal column based upon the above results.

#### 4-3 Foil reaction rate distribution in cavity

Reaction rates of gold foil  $^{197}\text{Au}$  ( $n, \gamma$ ), and indium foils  $^{115}\text{In}$  ( $n, n'$ ) and gold-cadmium ratio at the center of heavy concrete board beam hole plug surface (hole surface in case of "Without plug"), thermal column No. 25 duct inlet and fast column No. 26 duct inlet are shown in Table 4-1. Indium foil reaction rate at duct inlet was too low to detect. Beam holes and cavities of thermal column

and fast column are of the same dimensions and their streaming tendency is almost the same accordingly. At the reactor core, however, fast neutron flux of fast column side beam hole is low and its reaction rate is a little declined due to thick blanket.

Cadmium ratio at paraffin-contained plug beam hole outlet is nearly 10, which indicates that beams with many thermal neutrons are leaking into cavity. Cadmium ratio at duct inlet is, however, approximately 1.8, which does not greatly differ from those in cases of "Without plug" and "Aluminum plug". Taking this fact into account it may be presumed that, of ray flux components at duct inlet, those coming directly from beam hole outlet are few in number and that the flux components are almost those scattered by cavity wall.

#### 4-4 Measurement results by $\mu\text{BF}_3$ counter, of duct streaming

The measurement by  $\mu\text{BF}_3$  counter was conducted for three ducts, centering at No. 25 and No. 31 thermal column ducts and No. 26 fast column duct. These three ducts are different in point of positions in cavity, dimensions and forms. This measurement by  $\mu\text{BF}_3$  counter was performed on duct axis

from cavity floor face by means of a detector moving apparatus. Together with the results in cavity, representations were obtained as follows. Position at the height of more than  $H=150$  cm corresponds to duct interior.

Fig. 4-22 shows the comparison among the measurement results obtained on axes of ducts No. 23, No. 25 and No. 31 in case of "Without plug" using bare  $\mu\text{BF}_3$  counter. Damping in No. 31 duct shows a gradual slope. This is considered to have been caused by that as No. 31 duct is located nearby the heavy concrete wall the number of neutrons which are scattered there and injected toward duct axis is larger than those in No. 25 duct. Furthermore, diameters of No. 23 duct and No. 25 duct are increased from  $10\text{ cm}\phi$  to  $20\text{ cm}\phi$  at the point of 80 cm from the each duct inlet, making dampings there more gradual.

Fig. 4-23 represents plotted results of the counting rates per unit output of bare  $\mu\text{BF}_3$  counter at No. 25 duct. Irrespective of plugs, damping tendencies are almost the same. Paraffin-contained plug's damping seems, however, a little steeper, which is presumed to have been caused by softened spectrum. This is not so conspicuously different from other cases.

Fig. 4-24 and Fig. 4-25 show the comparison between bare  $\mu\text{BF}_3$  counter and cadmium-covered  $\mu\text{BF}_3$  in cases of "Aluminum plug" and "Paraffin-contained plug", respectively. The damping tendency is almost not affected by cadmium cover. In case of paraffin-contained plug, however, damping at the point where duct diameter is enlarged from 10 cm $\phi$  to 20 cm $\phi$  shows a little steepness, and remains the same in the enlarged portion of duct.

As is clear from Fig. 4-25, cadmium ratio by  $\mu\text{BF}_3$  counter varies in cavity with cases of "Without plug" and "Paraffin-contained plug", but they remains almost constant in the ducts.

The results of "Without plug" ducts No. 23 and No. 31 are given in Fig. 4-26 and Fig. 4-27, respectively. The damping of No. 23 duct is similar to that of No. 25 duct. Diameter of No. 31 duct remains at 10 cm, its damping becomes, however, slightly gradual as approaching the outlet.

The damping comparison by bare  $\mu\text{BF}_3$  counter between No. 25 duct and No. 31 duct in both case of "Aluminum plug" and "Paraffin-contained plug" is shown in Fig. 4-28 and Fig. 4-29. The difference in damping of ducts No. 25 and No. 31 is dependent upon the difference in duct shape and source

conditions as is stated in Fig. 4-22 regarding the case "Without plug". In case of "Paraffin-contained plug", damping in No. 31 duct shows a little steepness.

In addition, damping in No. 27 duct was similar to that in No. 25 duct, though not graphically represented.

Fig. 4-30 and Fig. 4-31 indicate the results about No. 26 duct on fast column side. The sectional area of No. 26 duct is 30 cm x 30 cm at its inlet and 46 cm x 46 cm at the point of 80 cm from its inlet, that is, its sectional area is large compared with thermal column side duct. This causes its gradual damping. The damping at the stepped portion does not vary so clearly as that of No. 25 duct.

In Fig. 4-32 is shown the comparison of damping between No. 25 duct and No. 26 duct in case of "Without plug".

#### 4-5 Measurement results by TLD, of duct streaming

First of all, the measurement results of gamma-ray dose is presented. Graphical representation is conducted taking the duct inlet from cavity as its original point.

The measurement results obtained in ducts No. 23, No. 25, No. 27 and No. 31 are given in Fig. 4-33, Fig. 4-34, Fig. 4-35 and Fig. 4-36, respectively. In case of "Paraffin-contained plug", damping tendency becomes somewhat steeper around the point of 80 cm and more from the duct inlet.

In Fig. 4-37 is indicated the comparison of damping between No. 23 duct and No. 31 duct as to the case of "Paraffin-contained plug".

The results of fast column at No. 26 duct is shown in Fig. 4-38. In this case too, damping in paraffin-contained plug gets a little steeper at the points apart from duct inlet by 80 cm and more like the above case.

Next, the measurement results of neutron reaction rate by means of  $^6\text{LiF}$  TLD is mentioned as follows.

In Fig. 4-39 is represented damping in No. 31 duct in the both cases of "Without plug" and "Paraffin-contained plug".

Fig. 4-40 shows dampings of ducts No. 23, No. 25 and No. 31 in case of "Paraffin-contained plug". Like the case of  $\mu\text{BF}_3$  counter, damping of No. 31 duct represents a little slowness.

Fig. 4-41 indicates the results obtained in No. 26 duct.

Damping comparison in No. 25 duct in case of "Without plug" is presented in Fig. 4-42. The measurement results of damping in duct by  $^6\text{LiF}$  TLD or by  $\mu\text{BF}_3$  counter are almost coincident with each other.

## 5. Summary of Experimental Results and its Consideration

The summary of the experimental results so far obtained is as follows:

- (1) Both the measurements by  $\mu\text{BF}_3$  counter and  $^6\text{LiF}$  TLD shows swelling in reaction rate around duct inlet.
- (2) As for gamma-ray, the above was not observed.
- (3) Both the distributions in cavity, of neutron and gamma-ray are symmetry as to beam axis, and reaction rate diminishes at wall side.
- (4) Gamma-ray distribution is flatter than that of neutron.
- (5) In the measurement by  $\mu\text{BF}_3$  counter, in ducts No. 23, No. 25 and No. 27, dampings within the ducts almost coincide with one another, irrespective of the existence of both plug and cadmium cover. In case of paraffin-contained plug,

however, damping varies a little around the point where duct diameter is enlarged to 20 cm $\phi$ . This tendency covers all the enlarged duct portion.

(6) Damping in duct is exponential, and varies with the change of duct diameter.

(7) In the both cases of "Without plug" and "Paraffin-contained plug", cadmium ratio of  $\mu\text{BF}_3$  varies in cavity, but it remains almost the same in duct.

(8) When paraffin-contained plug is stuffed, cadmium ratio (gold foil) approaches nearly 10 at beam's outlet to cavity and beam comes to have many thermal neutrons. At the inlet of No. 25 duct, however, cadmium ratio decreases considerably.

(9) Regarding neutron reaction rate, the two results by  $^6\text{LiF}$  TLD and by  $\mu\text{BF}_3$  counter are almost equal in the point of relative values.

From the experimental summary described above, the following facts were noticed for the case where beam-formed neutrons leak with cavity-like form as the reactor "YAYOI":

a) The distribution form at around beam outlet varies with depending upon the existence of scatterers at the beam outlet.

b) The influence by spectrum of injection beam is lessened, however, due to the scattering

result in cavity, and dampings in the ducts leading to cavity show the almost similar tendency.

c) Such dampings in ducts are also exponential.

This damping differs from inverse square damping of the well-known direct-vision component distance as well as from inverse triplicate damping<sup>(1)</sup> that is said to be formed at  $5 < Z/r < 30$  with epithermal neutron in straight cylindrical duct.  $Z$ ,  $r$  represent length and radius of duct, respectively.

The comparison about the above is shown in Fig. 5-1 regarding No. 25 duct.

Damping is not represented by the direct-vision component, probably because of the great contribution of component that reaches duct through heavy concrete wall after the scattering on cavity wall.

## 6. Conclusion

With regard to the structural system where streaming occurs in duct through cavity, the experimental data was obtained taking duct diameter and injection spectrum into cavity as parameter. From this data, it has become evident that damping in duct is not so

dependent upon injection spectrum by dint of scattering in cavity.

## 7. Figures and Tables

Fig. 2-1 Experimental configuration

Fig. 2-2 Core structure of Reactor "YAYOI"

Fig. 4-1 TLD measurement position at thermal column cavity; H: Height from cavity floor, D: Distance from cavity inlet face, L: Distance from cavity side face

Fig. 4-2 Neutron reaction rate distribution in thermal column cavity by  $^6\text{LiF}$  TLD (Without plug; H=150, 125 cm)

Fig. 4-3 Neutron reaction rate distribution in thermal column cavity by  $^6\text{LiF}$  TLD (Al plug; H=150, 125 cm)

Fig. 4-4 Neutron reaction rate distribution in thermal column cavity by  $^6\text{LiF}$  TLD (Paraffin-contained plug, H=150, 125 cm)

Fig. 4-5 Neutron reaction rate distribution in thermal column cavity by  $^6\text{LiF}$  TLD (Without plug; H=75, 100, 125 cm)

Fig. 4-6 Neutron reaction rate distribution in thermal column cavity by  $^6\text{LiF}$  TLD (Paraffin-contained plug; H=75, 100, 125 cm)

- Fig. 4-7 Gamma-ray dose rate distribution in thermal column cavity by TLD (Without plug; H=75, 100, 125, 150 cm)
- Fig. 4-8 Gamma-ray dose rate distribution in thermal column cavity by TLD (Al plug; H=75, 100, 125, 137.5 cm)
- Fig. 4-9 Gamma-ray dose rate distribution in thermal column cavity by TLD (Paraffin-contained plug; H=100, 125, 150 cm)
- Fig. 4-10 Neutron reaction rate distribution in thermal column cavity by  $^6\text{LiF}$  TLD (Without plug; on line represented by L=75 cm and H=75 cm on face of D=87.5 cm)
- Fig. 4-11 Neutron reaction rate distribution in thermal column cavity by  $^6\text{LiF}$  TLD (Paraffin-contained plug; on line represented by L=75 cm and H=75 cm on face of D=87.5 cm)
- Fig. 4-12 Neutron reaction rate distribution in fast column cavity (Without plug; H=75, 100, 125, 150 cm)
- Fig. 4-13 Neutron reaction rate distribution in fast column cavity (Al plug; H=75, 100, 125, 150 cm)
- Fig. 4-14 Neutron reaction rate distribution in fast column cavity (Paraffin-contained plug; H=75, 100, 125, 150 cm)

- Fig. 4-15 Gamma-ray dose rate distribution (Without plug; H=75, 100, 125, 150 cm)
- Fig. 4-16 Gamma-ray dose rate distribution in fast column cavity by TLD (Al plug; H=75, 100, 125, 150 cm)
- Fig. 4-17 Gamma-ray dose rate distribution in fast column cavity by TLD (Paraffin-contained plug; H=75, 100, 125, 150 cm)
- Fig. 4-18 Neutron counting rate distribution in thermal column cavity by  $\mu\text{BF}_3$  counter (Without plug; Upper figure — with Cd cover, Lower figure — without cover)
- Fig. 4-19 Neutron counting rate distribution in thermal column cavity by  $\mu\text{BF}_3$  counter (Al plug; Upper figure — with Cd cover, Lower figure — without cover)
- Fig. 4-20 Neutron counting rate distribution in thermal column cavity by  $\mu\text{BF}_3$  counter (Paraffin-contained plug; Upper figure — with Cd cover, Lower figure — without cover)
- Fig. 4-21 Neutron counting rate distribution in thermal column cavity by  $\mu\text{BF}_3$  counter
- Table 4.1 Reaction rate distributions and cadmium ratios in the cavities by gold foils and indium foils

- Fig. 4-22 Neutron counting rate (Without plug) on duct axes of No. 23, No. 25, No. 31 by  $\mu\text{BF}_3$  counter (bare)
- Fig. 4-23 Neutron counting rate on No. 25 duct axis by  $\mu\text{BF}_3$  counter (bare) — "Without plug", "Al plug", "Paraffin-contained plug"
- Fig. 4-24 Neutron counting rate of  $\mu\text{BF}_3$  counter on No. 25 duct axis — "Without plug", "Al plug"
- Fig. 4-25 Neutron counting rate of  $\mu\text{BF}_3$  counter on No. 25 duct axis — "Without plug", "Paraffin-contained plug"
- Fig. 4-26 Neutron counting rate distribution of  $\mu\text{BF}_3$  counter on No. 23 duct — "Without plug"
- Fig. 4-27 Neutron counting rate distribution of  $\mu\text{BF}_3$  counter on No. 31 duct axis — "Without plug"
- Fig. 4-28 Neutron counting rate on duct axes of No. 25, No. 31 by  $\mu\text{BF}_3$  counter — "Al plug"
- Fig. 4-29 Neutron counting rate on duct axes of No. 25, No. 31 by  $\mu\text{BF}_3$  counter — "Paraffin-coated plug"
- Fig. 4-30 Neutron counting rate on No. 26 duct axis by  $\mu\text{BF}_3$  counter — "Without plug", "Paraffin-contained plug"
- Fig. 4-31 Neutron counting rate on No. 26 duct axis — "Al plug"

- Fig. 4-32 Neutron counting rate on duct axes of No. 25, No. 26 by  $\mu\text{BF}_3$  counter — "Without plug"
- Fig. 4-33 Gamma-ray dose rate in No. 23 duct by TLD — "Without plug", "Al plug", "Paraffin-contained plug"
- Fig. 4-34 Gamma-ray dose rate in No. 25 duct by TLD — "Without plug", "Al plug", "Paraffin-contained plug"
- Fig. 4-35 Gamma-ray dose rate in No. 27 duct by TLD — "Without plug", "Al plug", "Paraffin-contained plug"
- Fig. 4-36 Gamma-ray dose rate in No. 31 duct by TLD — "Without plug", "Al plug", "Paraffin-contained plug"
- Fig. 4-37 Gamma-ray dose rate in ducts of No. 23, No. 31 by TLD — "Paraffin-contained plug"
- Fig. 4-38 Gamma-ray dose rate in No. 26 duct by TLD — "Without plug", "Al plug", "Paraffin-contained plug"
- Fig. 4-39 Neutron reaction rate in No. 31 duct by  $^6\text{LiF}$  TLD — "Without plug", "Paraffin-contained plug"
- Fig. 4-40 Neutron reaction rate in ducts of No. 23, No. 25, No. 31 by  $^6\text{LiF}$  TLD — "Paraffin-contained plug"

Fig. 4-41 Neutron reaction rate in No. 26 duct by  
 $^6\text{LiF}$  TLD — "Without plug", "Al plug",  
"Paraffin-contained plug"

Fig. 4-42 Comparison among neutron reaction rate by  
 $^6\text{LiF}$  TLD, neutron counting rate by  $\mu\text{BF}_3$   
counter, gamma-ray dose rate by TLD in  
No. 25 duct — "Without plug"

Fig. 5-1 Comparison between non-dimensional damping  
in No. 25 duct and analysis formula (Neu-  
tron counting rate by  $\mu\text{BF}_3$  counter —  
"Without plug")



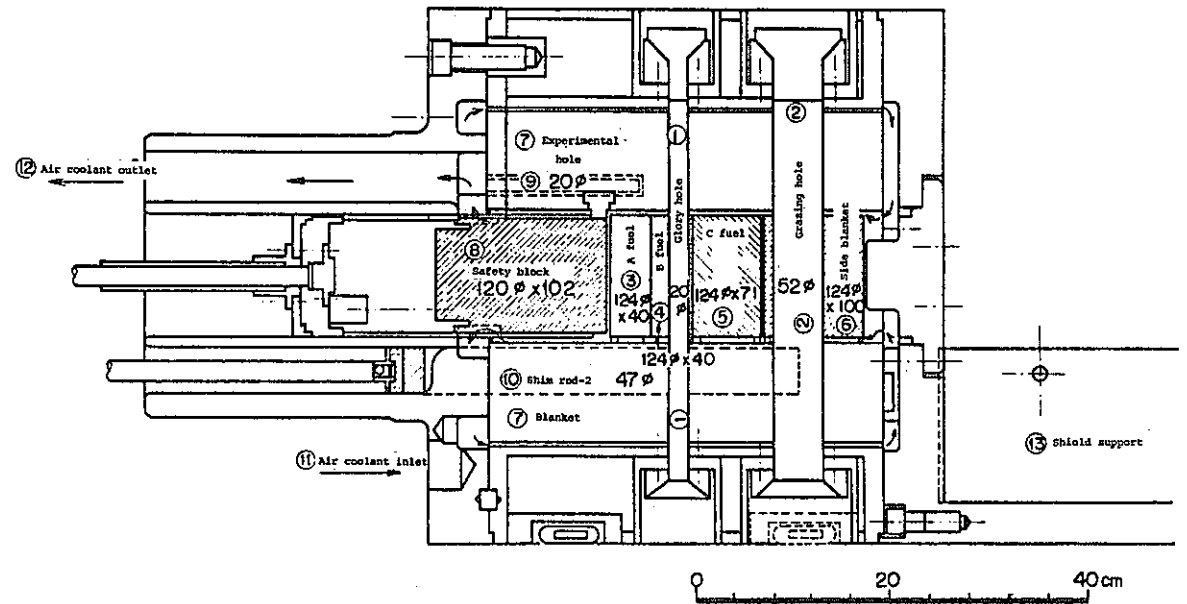
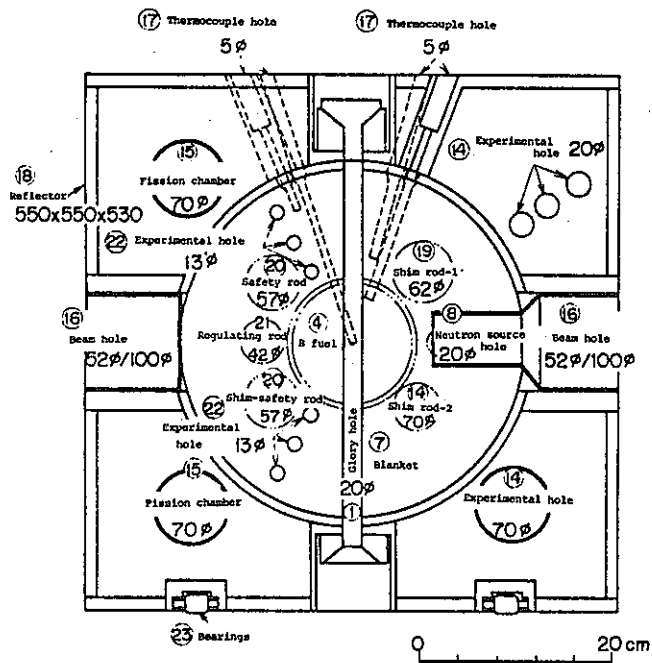


Fig. 2-2 Core structure of Reactor "YAYOI"

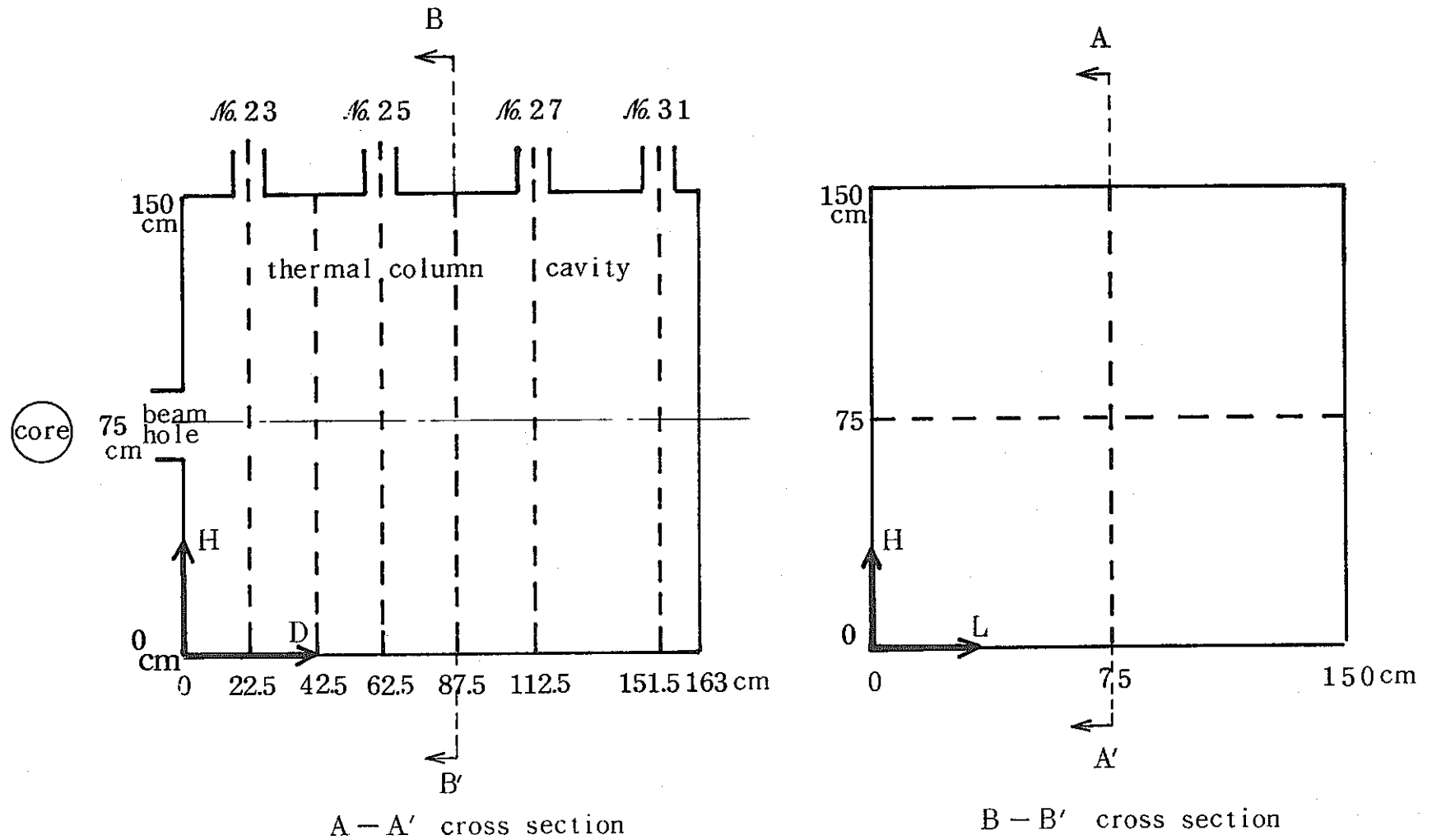


Fig. 4-1 TLD measurement position at thermal column cavity; H: Height from cavity floor, D: Distance from cavity inlet face, L: Distance from cavity side face

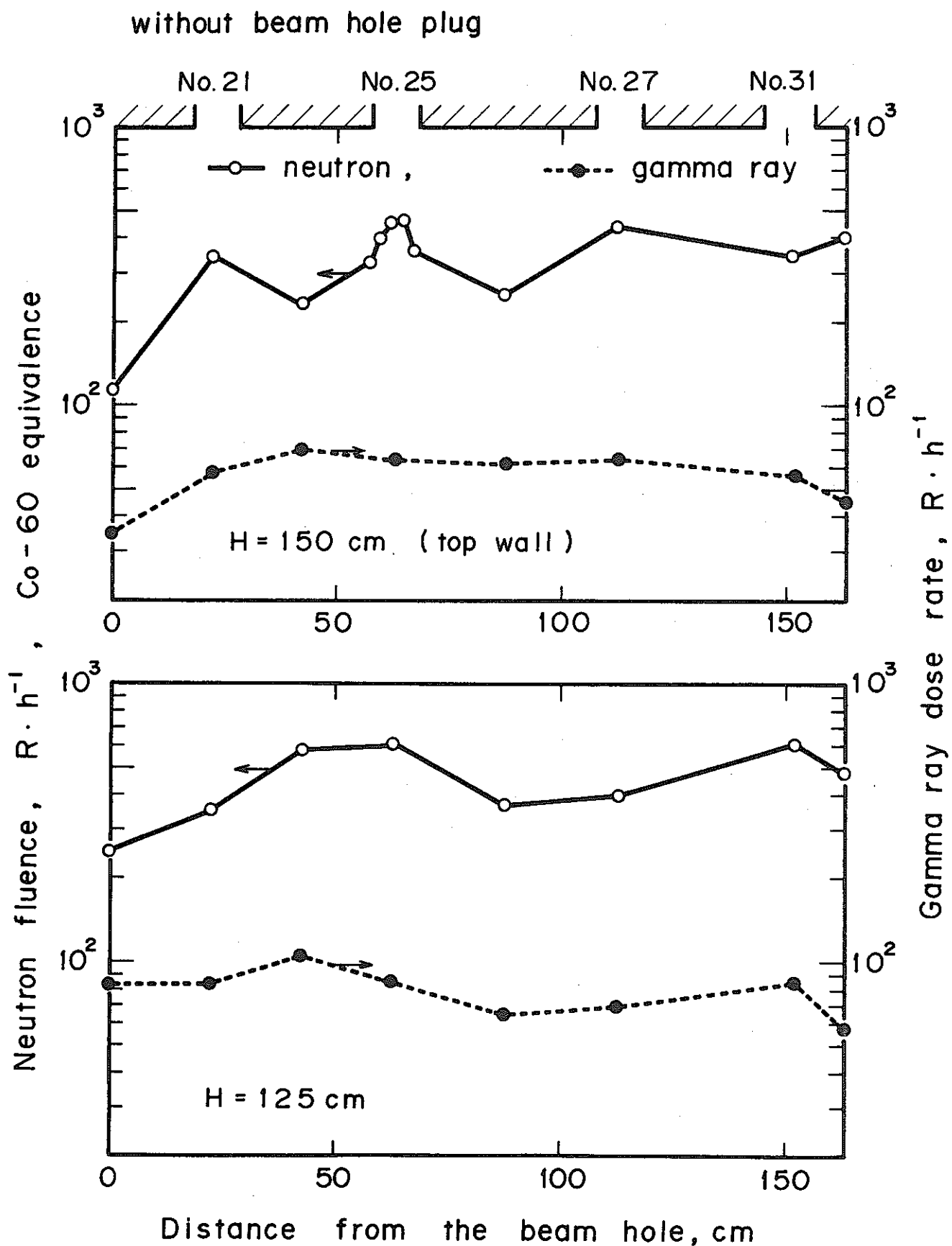


Fig. 4-2 Neutron reaction rate distribution in thermal column cavity by  $^6\text{LiF}$  TLD (Without plug; H=150, 125 cm)

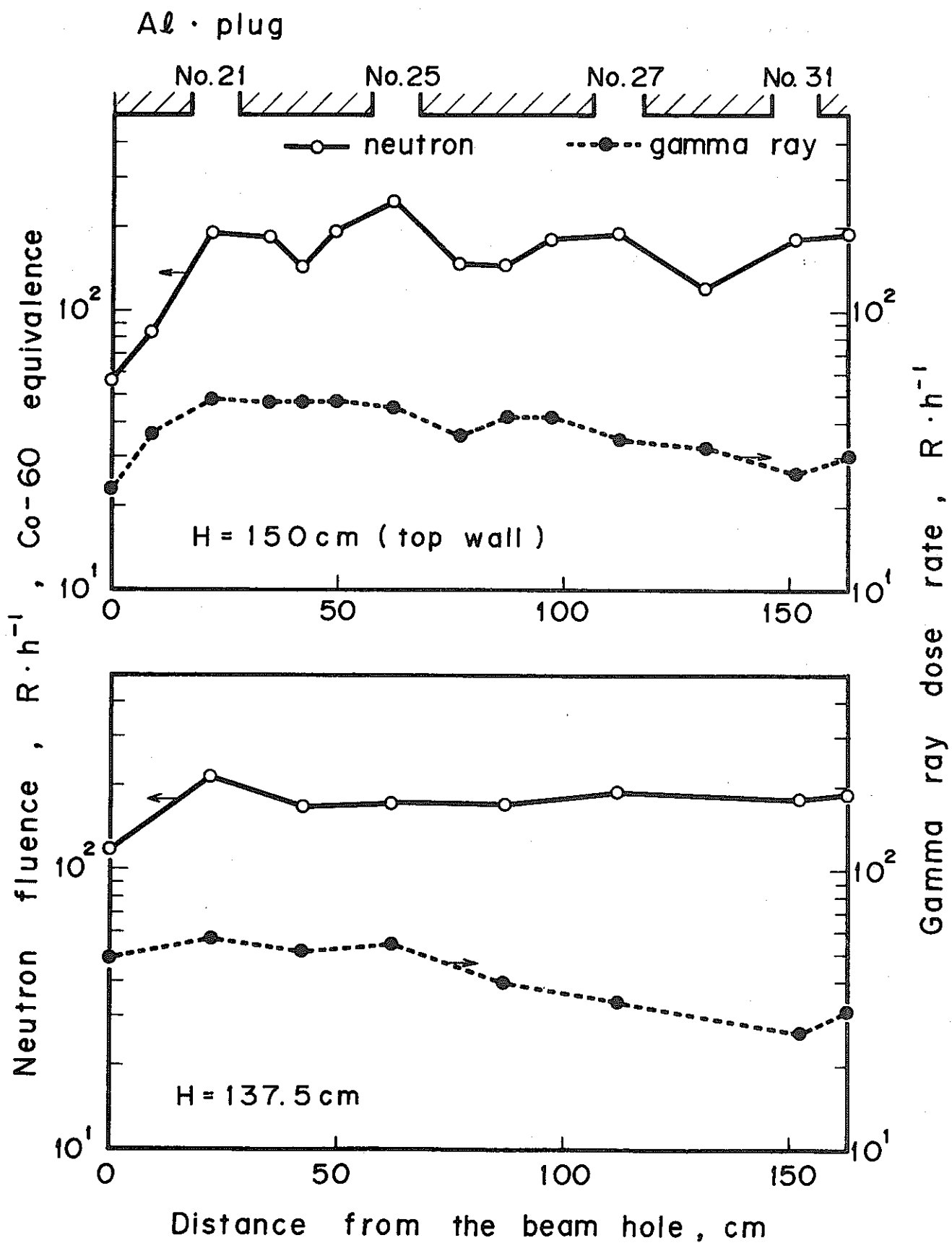


Fig. 4-3 Neutron reaction rate distribution in thermal column cavity by  $^6\text{LiF}$  TLD (Al plug; H-150, 125 cm)

Pb + C + Paraffin plug

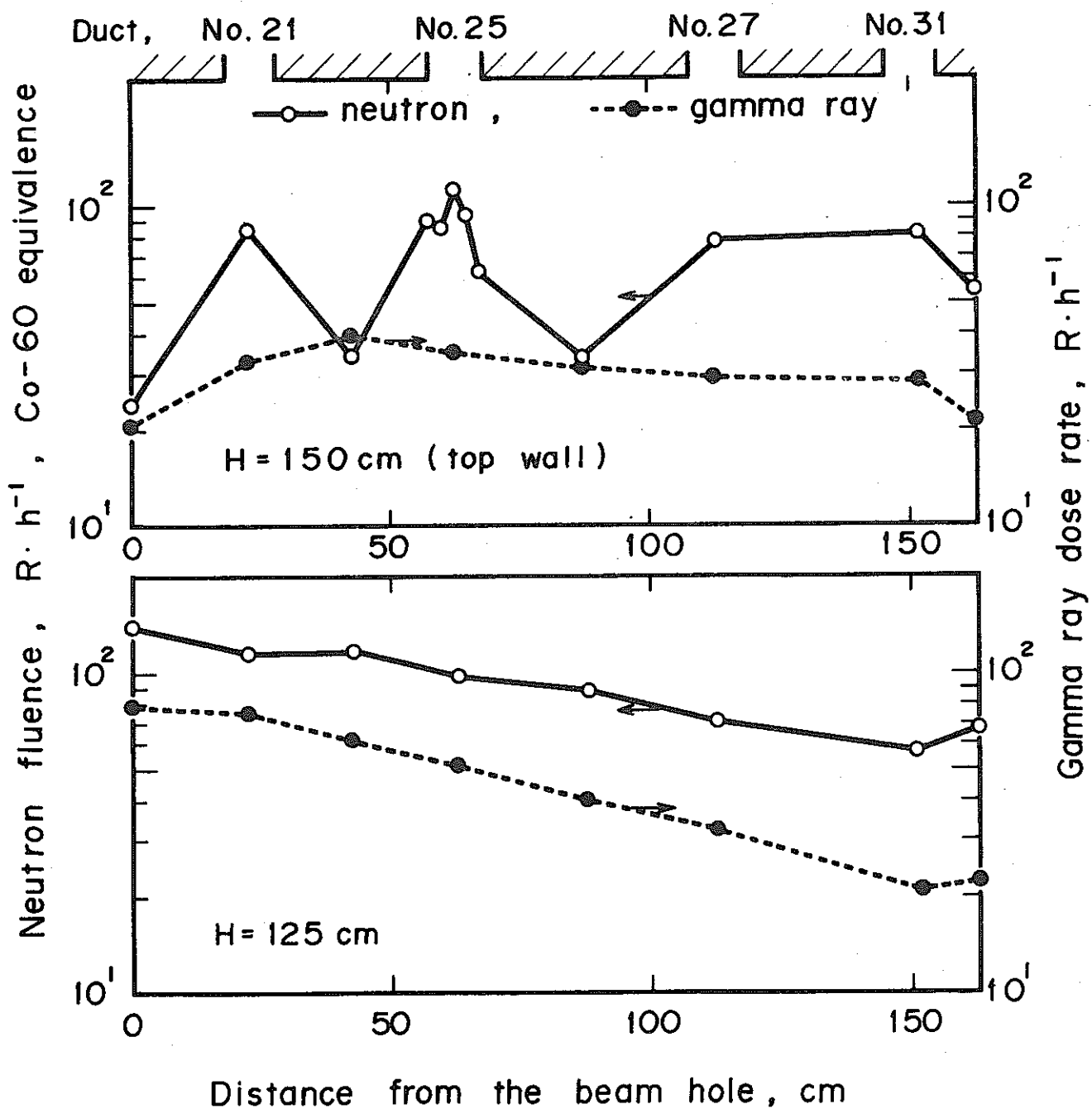


Fig. 4-4 Neutron reaction rate distribution in thermal column cavity by  $^6\text{LiF}$  TLD (Paraffin-contained plug,  $H=150, 125 \text{ cm}$ )

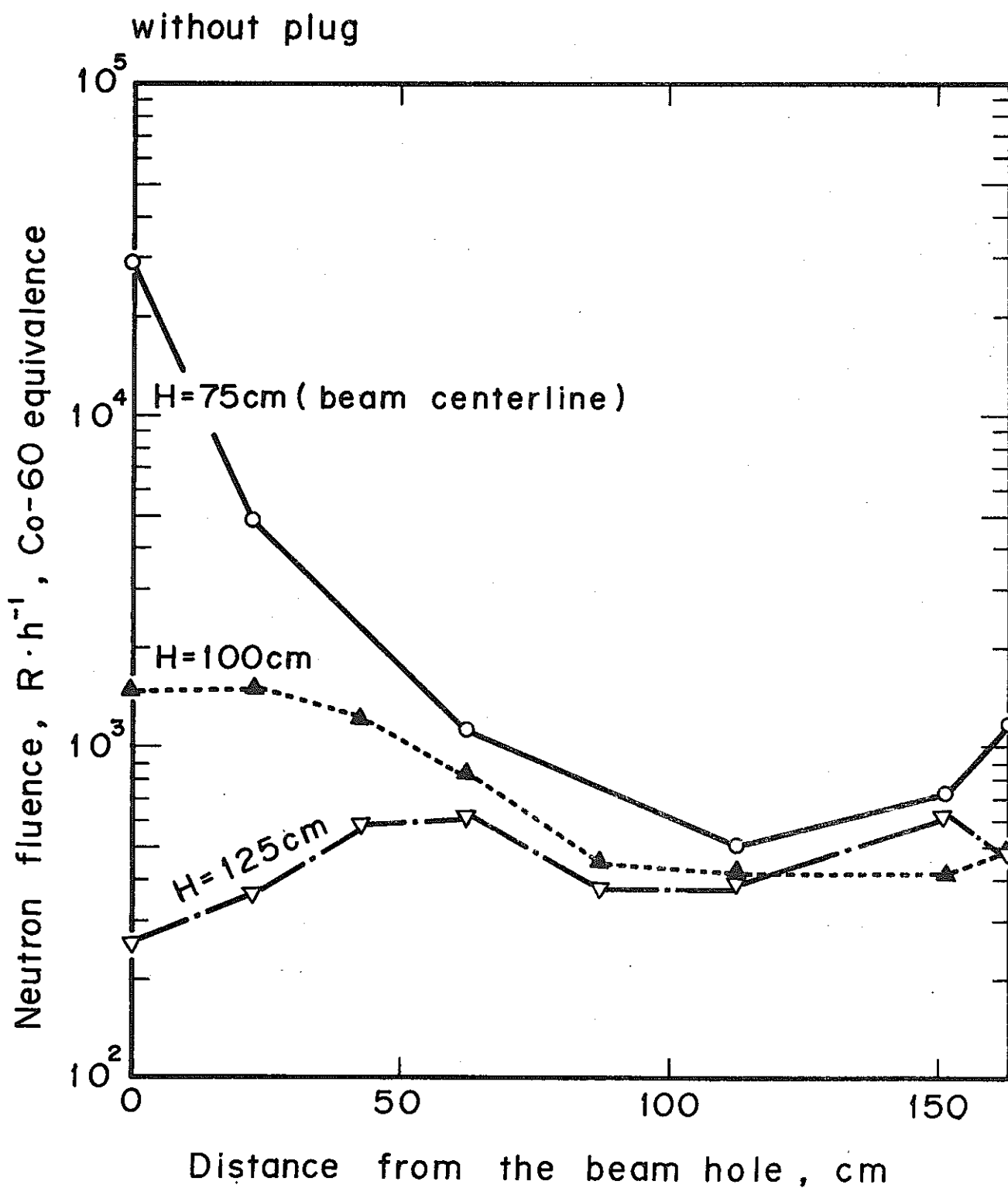


Fig. 4-5 Neutron reaction rate distribution in thermal column cavity by  $^6\text{LiF}$  TLD (Without plug;  $H=75, 100, 125$  cm)

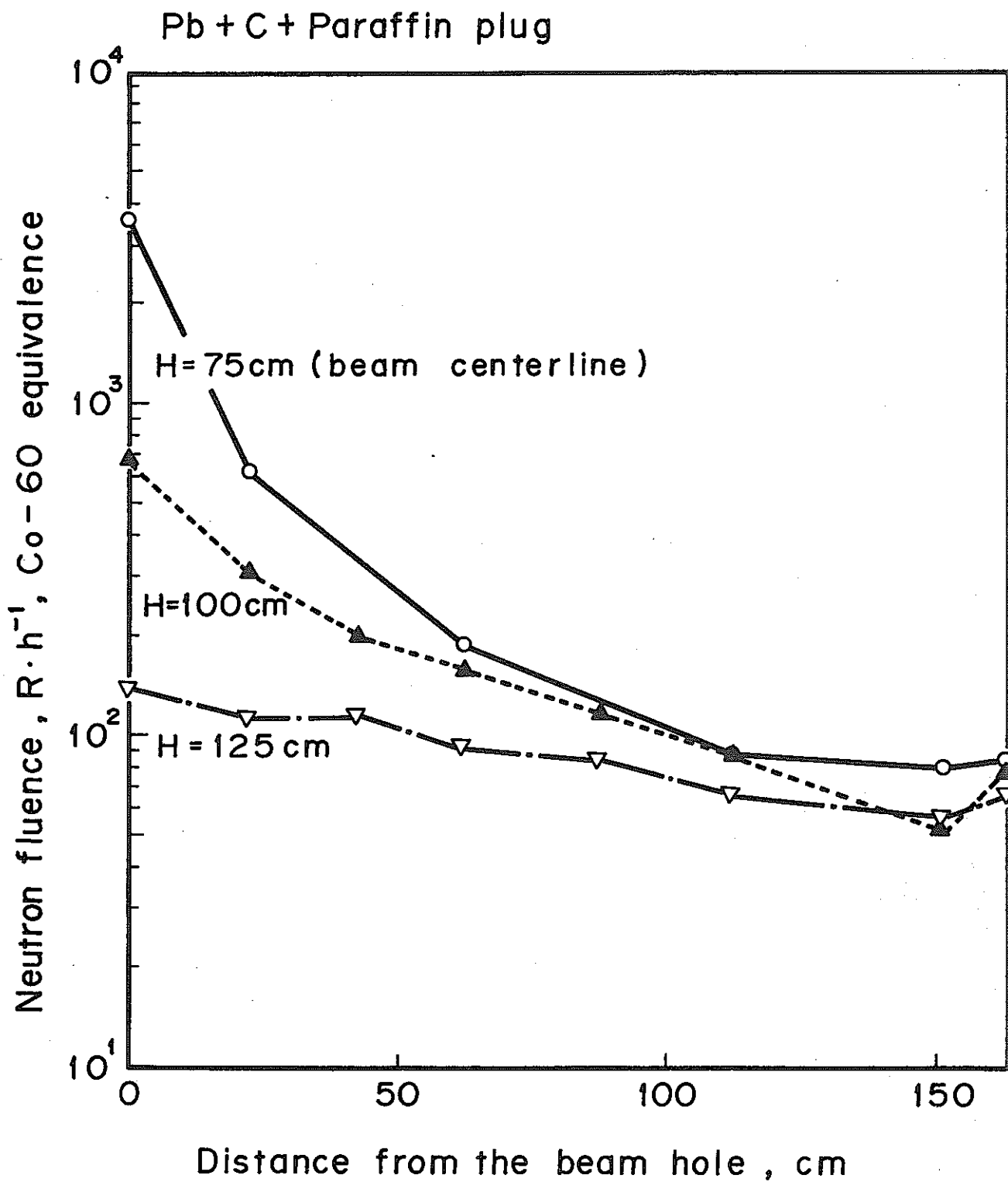


Fig. 4-6 Neutron reaction rate distribution in thermal column cavity by  ${}^6\text{LiF}$  TLD (Paraffin-contained plug; H=75, 100, 125 cm)

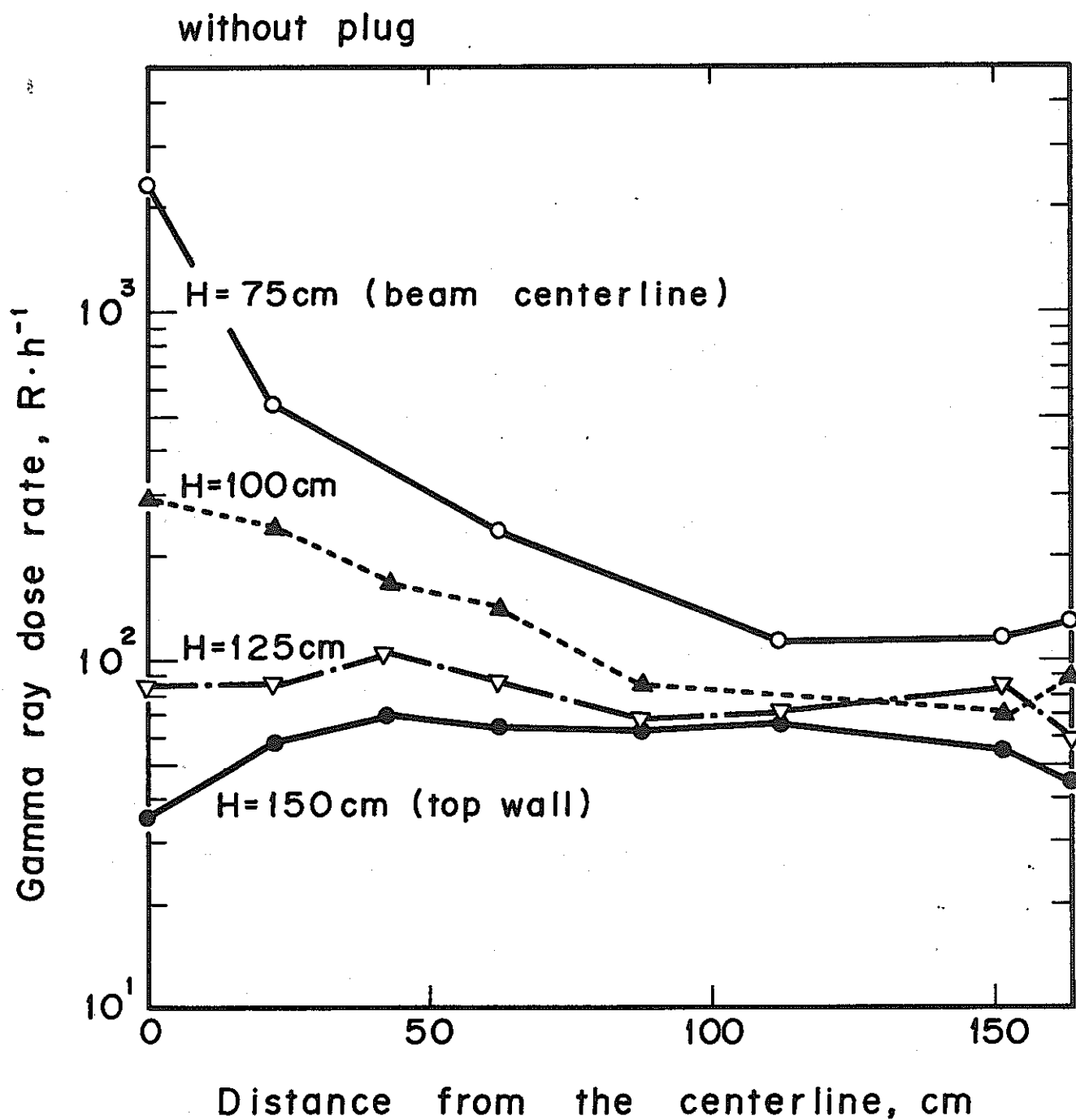


Fig. 4-7 Gamma-ray dose rate distribution in thermal column cavity by TLD (Without plug; H=75, 100, 125, 150 cm)

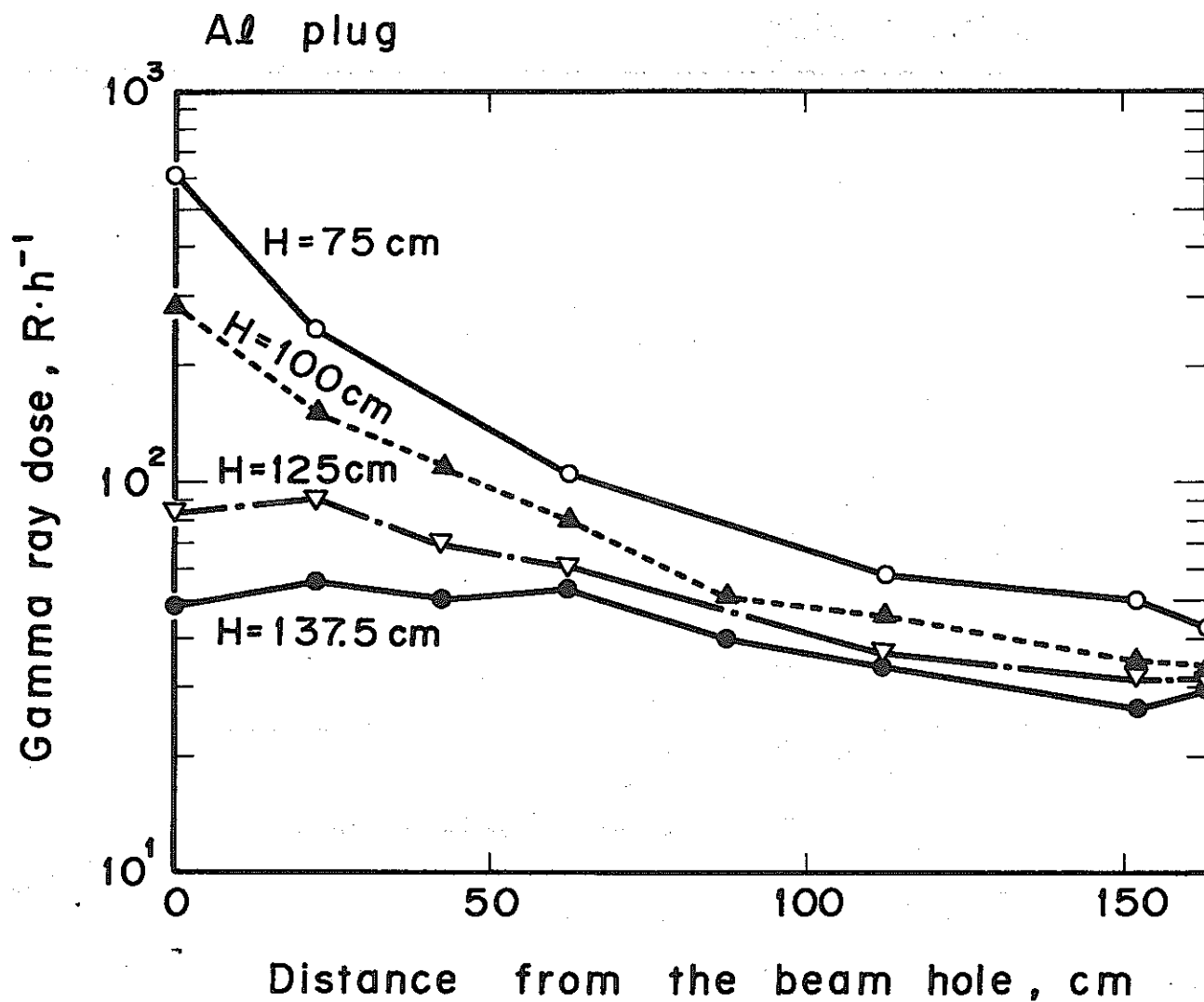


Fig. 4-8 Gamma-ray dose rate distribution in thermal column cavity by TLD (Al plug;  $H=75$ , 100, 125, 137.5 cm)

# Pb + C + Paraffin plug

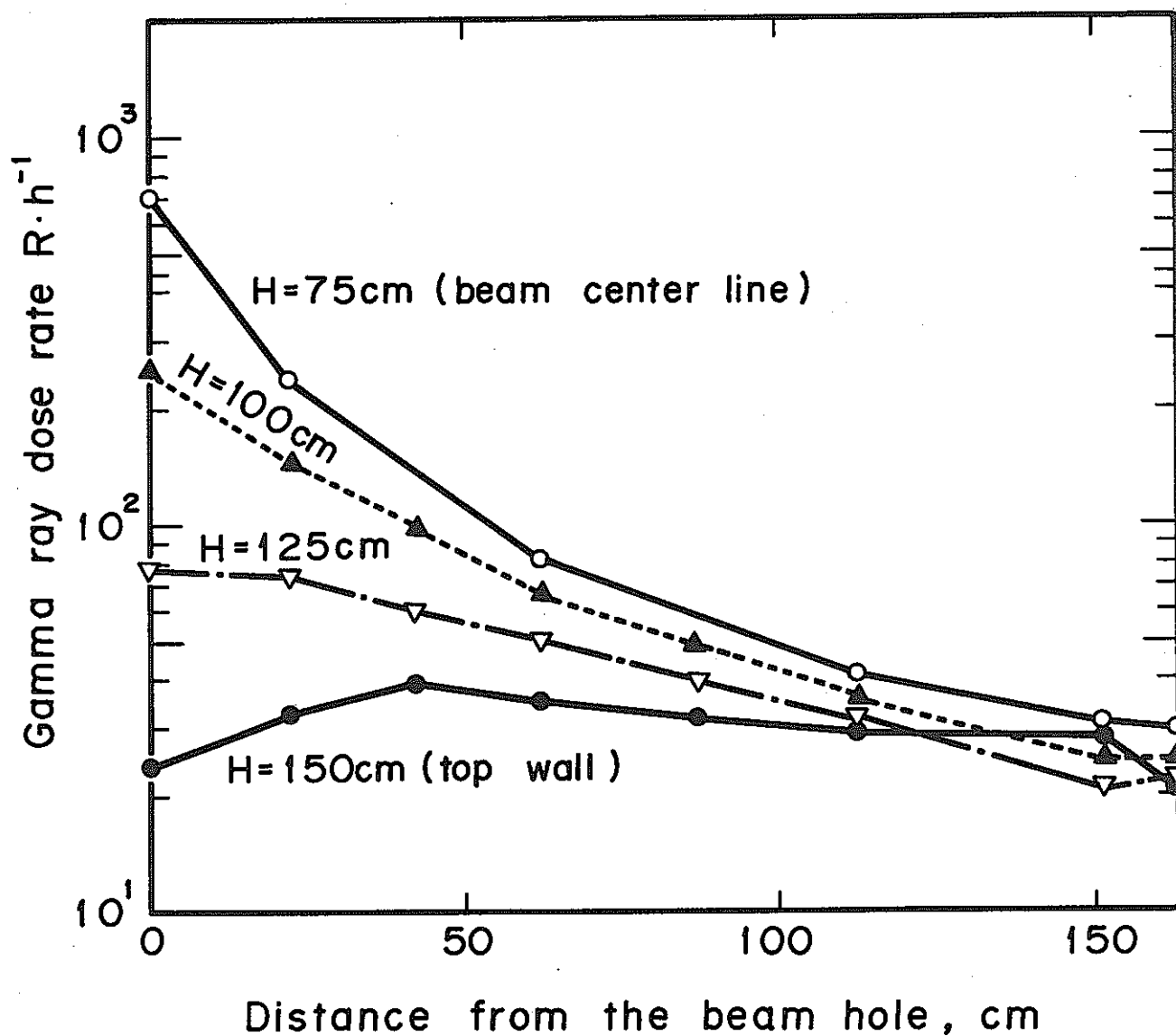


Fig. 4-9 Gamma-ray dose rate distribution in thermal column cavity by TLD (Paraffin-contained plug; H=100, 125, 150 cm)

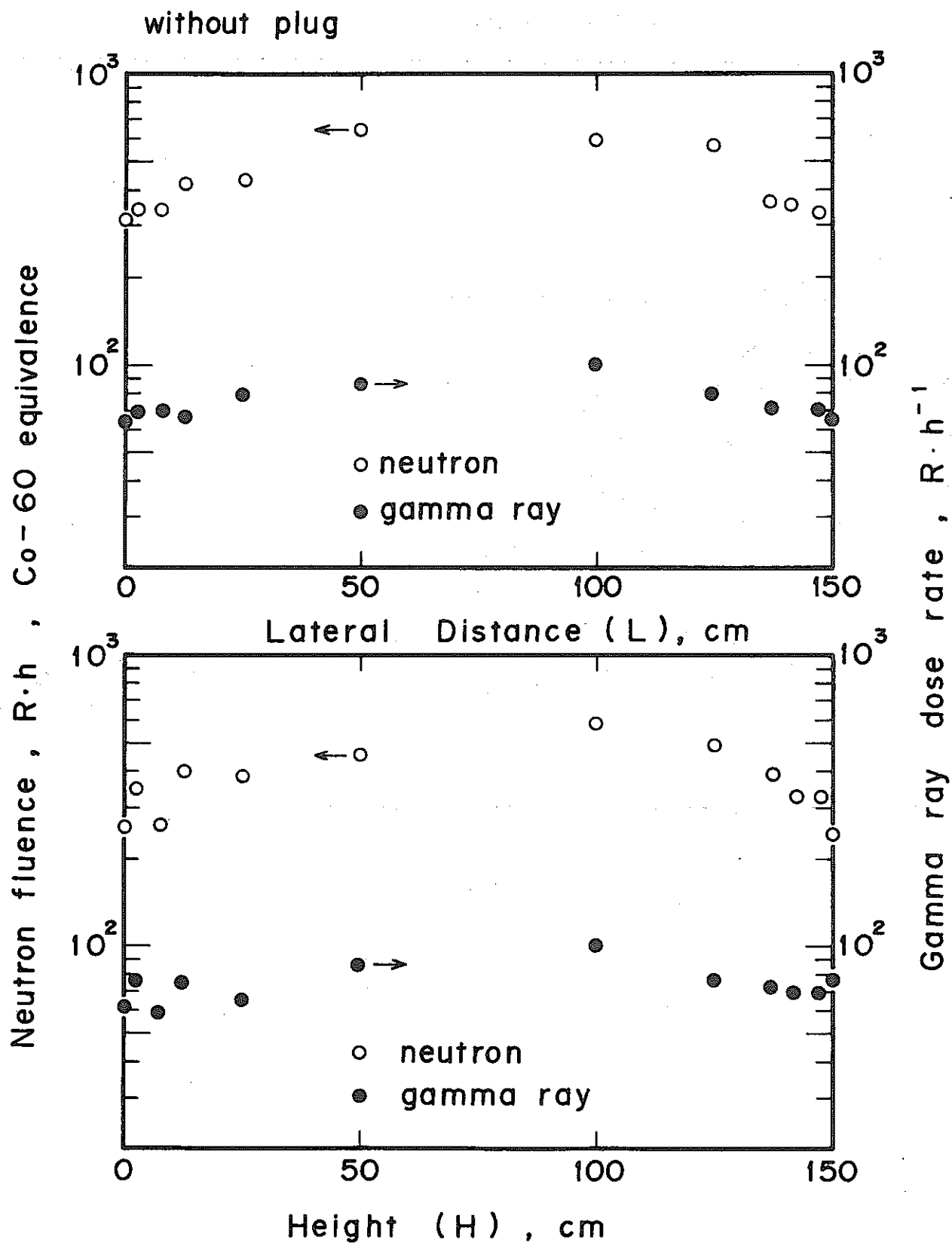


Fig. 4-10 Neutron reaction rate distribution in thermal column cavity by  $^6\text{LiF}$  TLD (Without plug; on line represented by  $L=75$  cm and  $H=75$  cm on face of  $D=87.5$  cm)

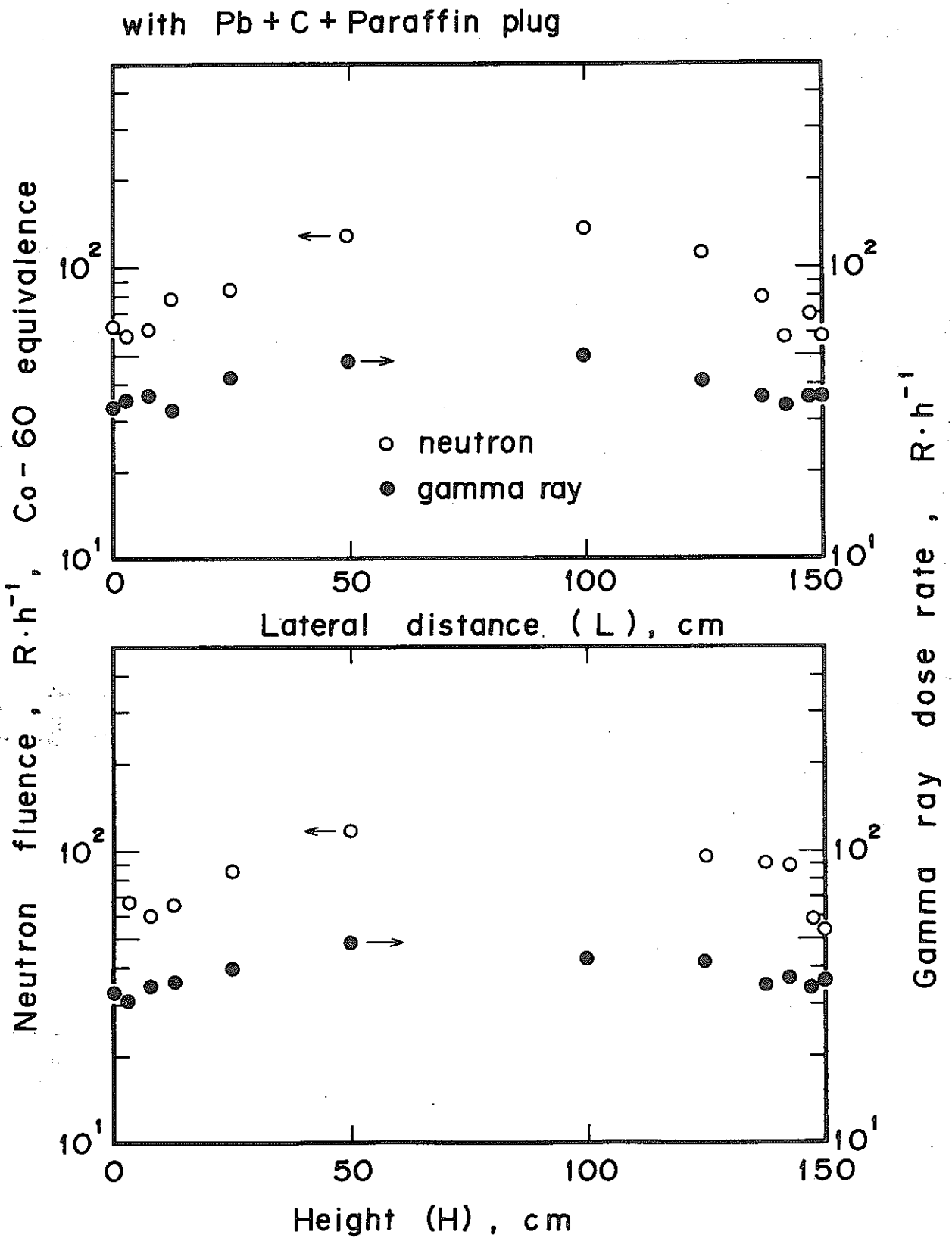


Fig. 4-11 Neutron reaction rate distribution in thermal column cavity by  $^6\text{LiF}$  TLD (Paraffin-contained plug; on line represented by  $L=75$  cm and  $H=75$  cm on face of  $D=87.5$  cm)

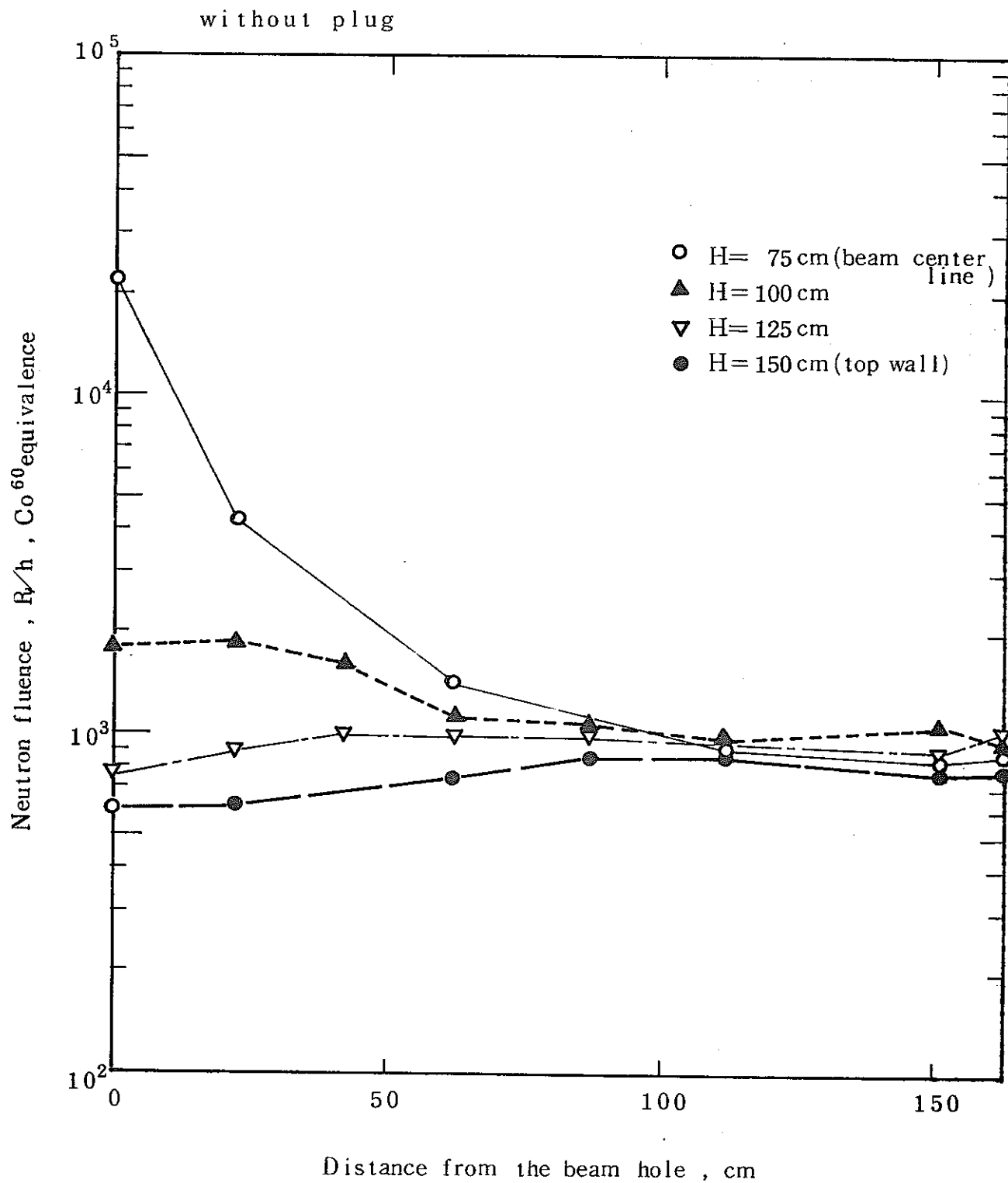


Fig. 4-12 Neutron reaction rate distribution in fast column cavity (Without plug;  $H=75, 100, 125, 150$  cm)

Al plug

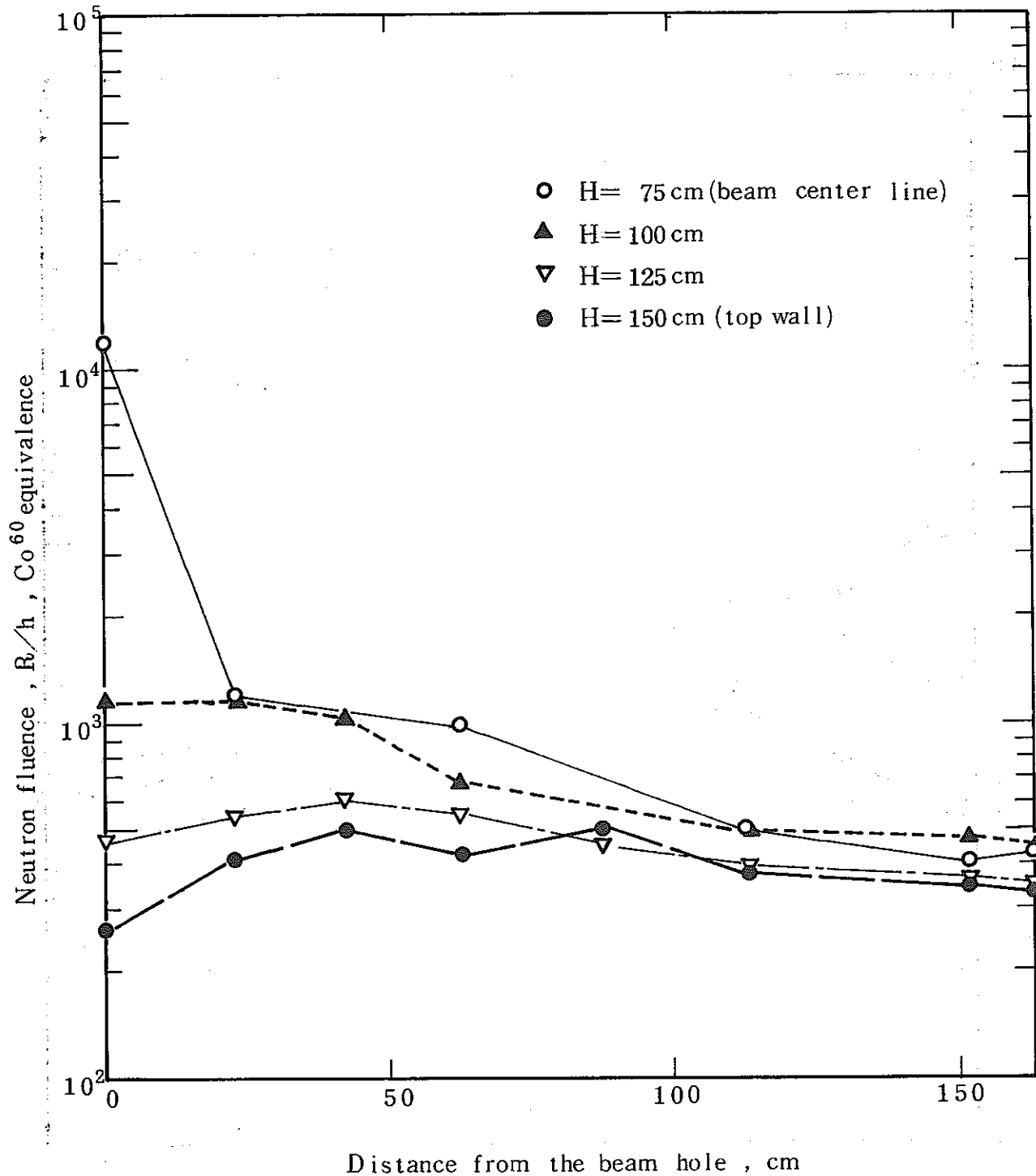


Fig. 4-13 Neutron reaction rate distribution in fast column cavity (Al plug; H=75, 100, 125, 150 cm)

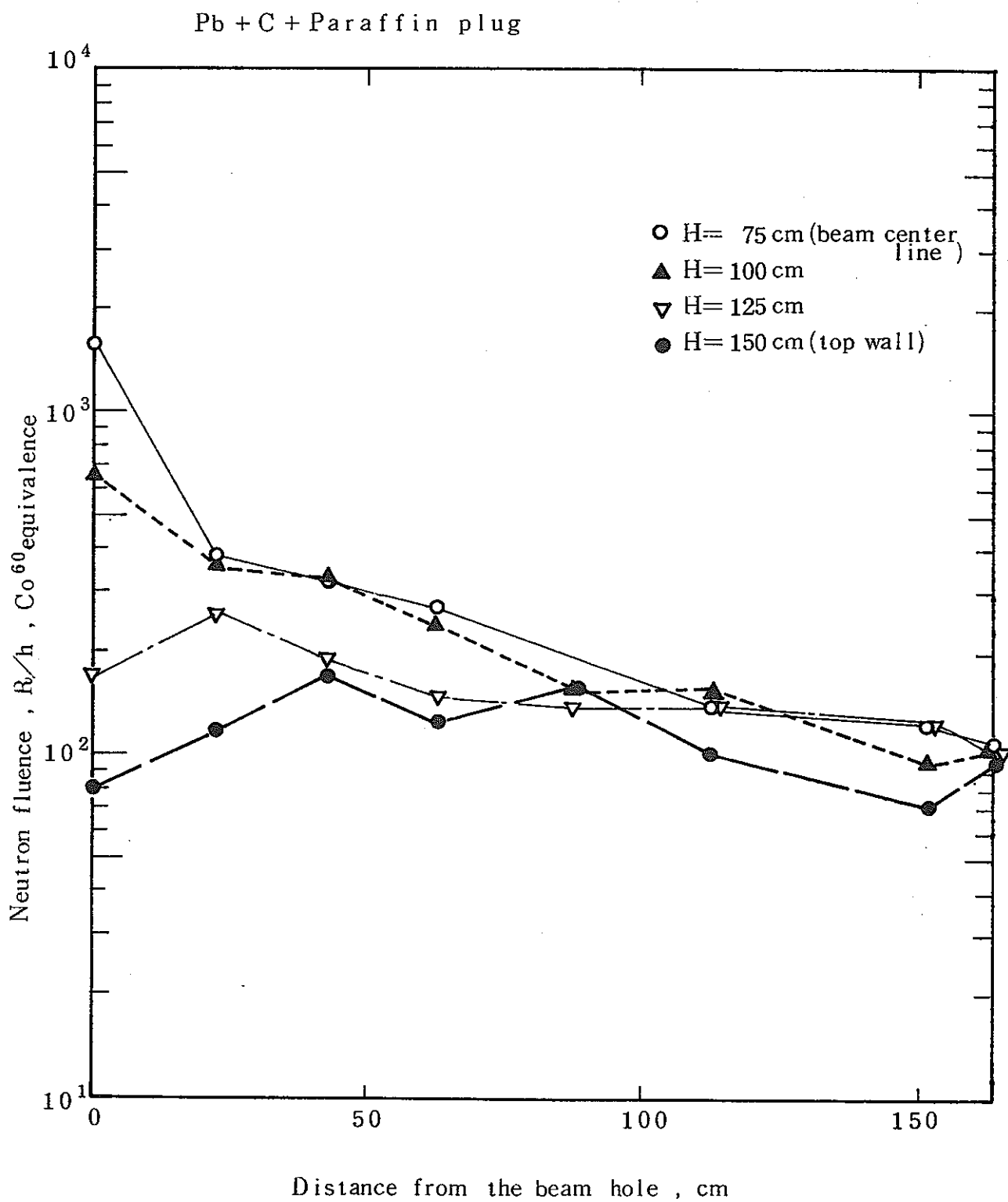


Fig. 4-14 Neutron reaction rate distribution in fast column cavity (Paraffin-contained plug;  $H=75, 100, 125, 150$  cm)

Without plug

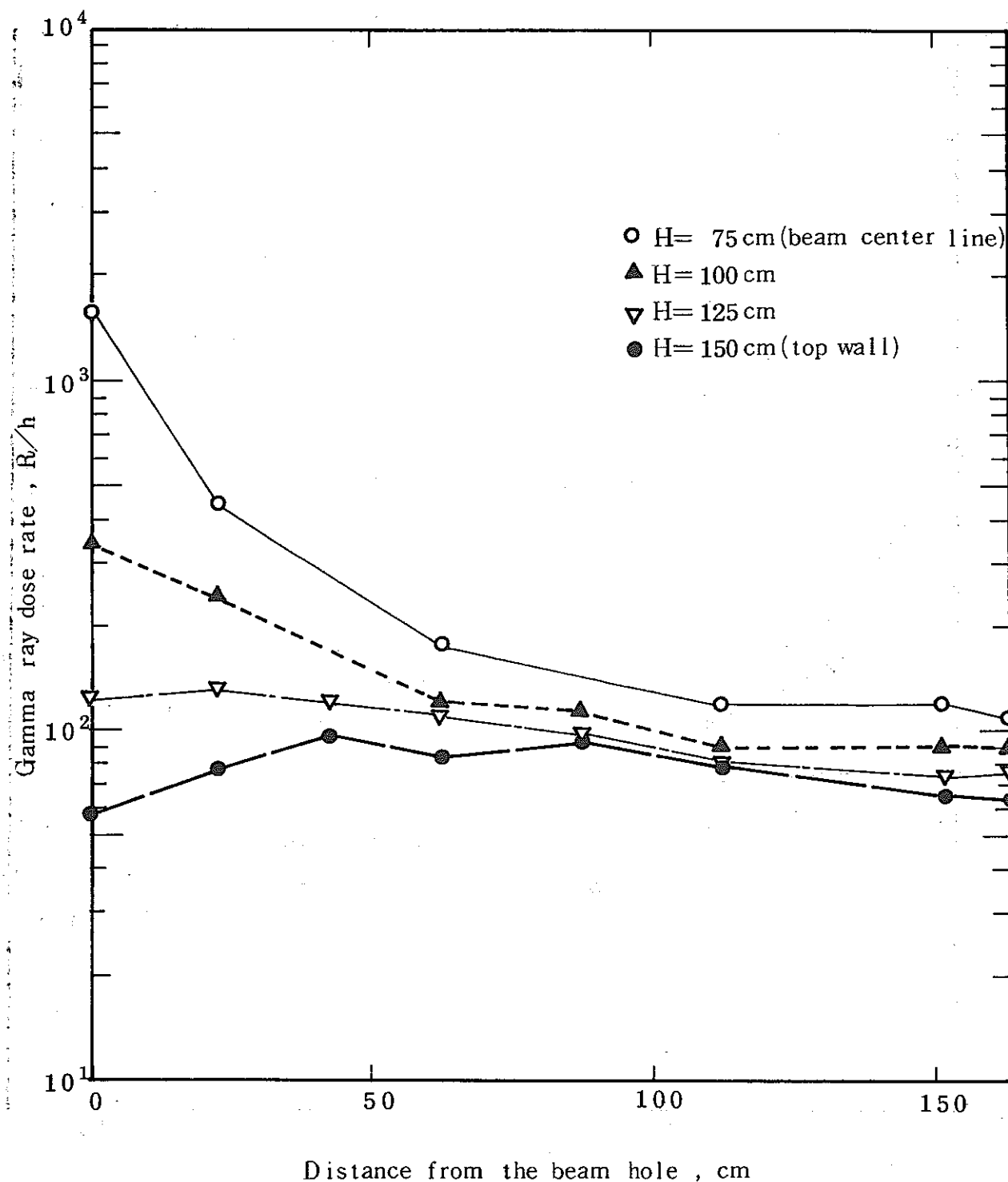


Fig. 4-15 Gamma-ray dose rate distribution (Without plug;  $H=75, 100, 125, 150$  cm)

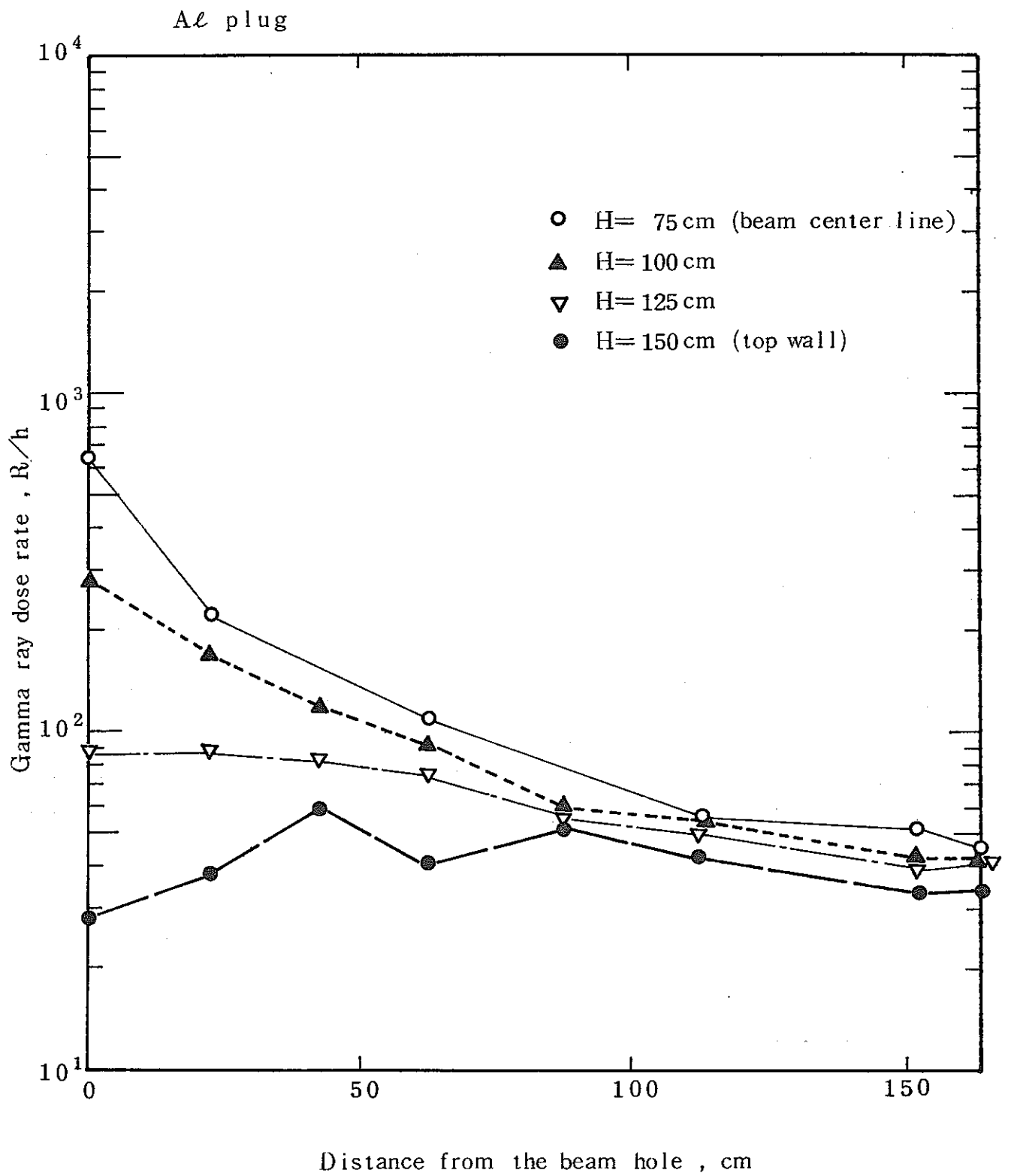


Fig. 4-16 Gamma-ray dose rate distribution in fast column cavity by TLD (Al plug;  $H=75, 100, 125, 150$  cm)

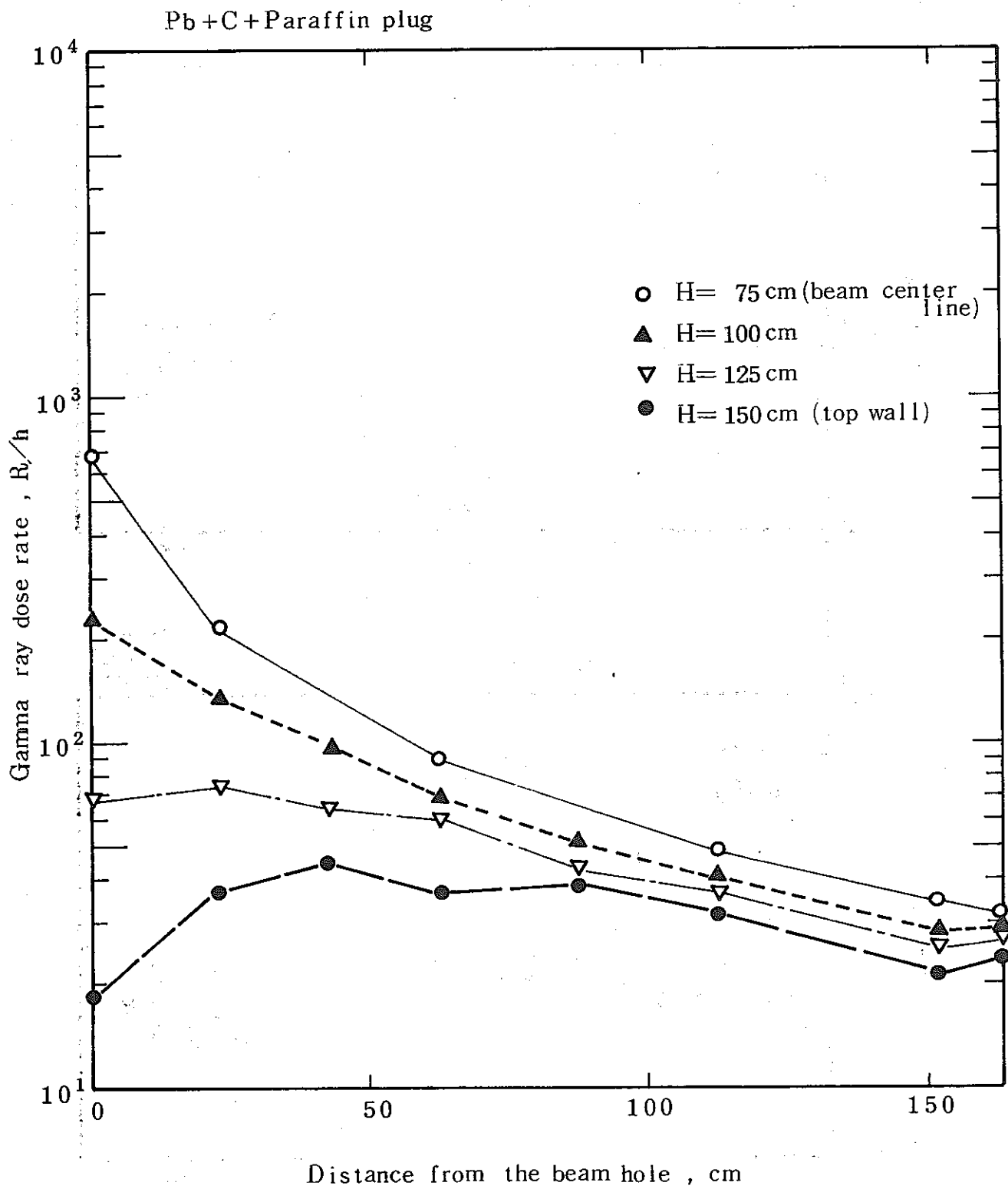


Fig. 4-17 Gamma-ray dose rate distribution in fast column cavity by TLD (Paraffin-contained plug;  $H=75, 100, 125, 150$  cm)

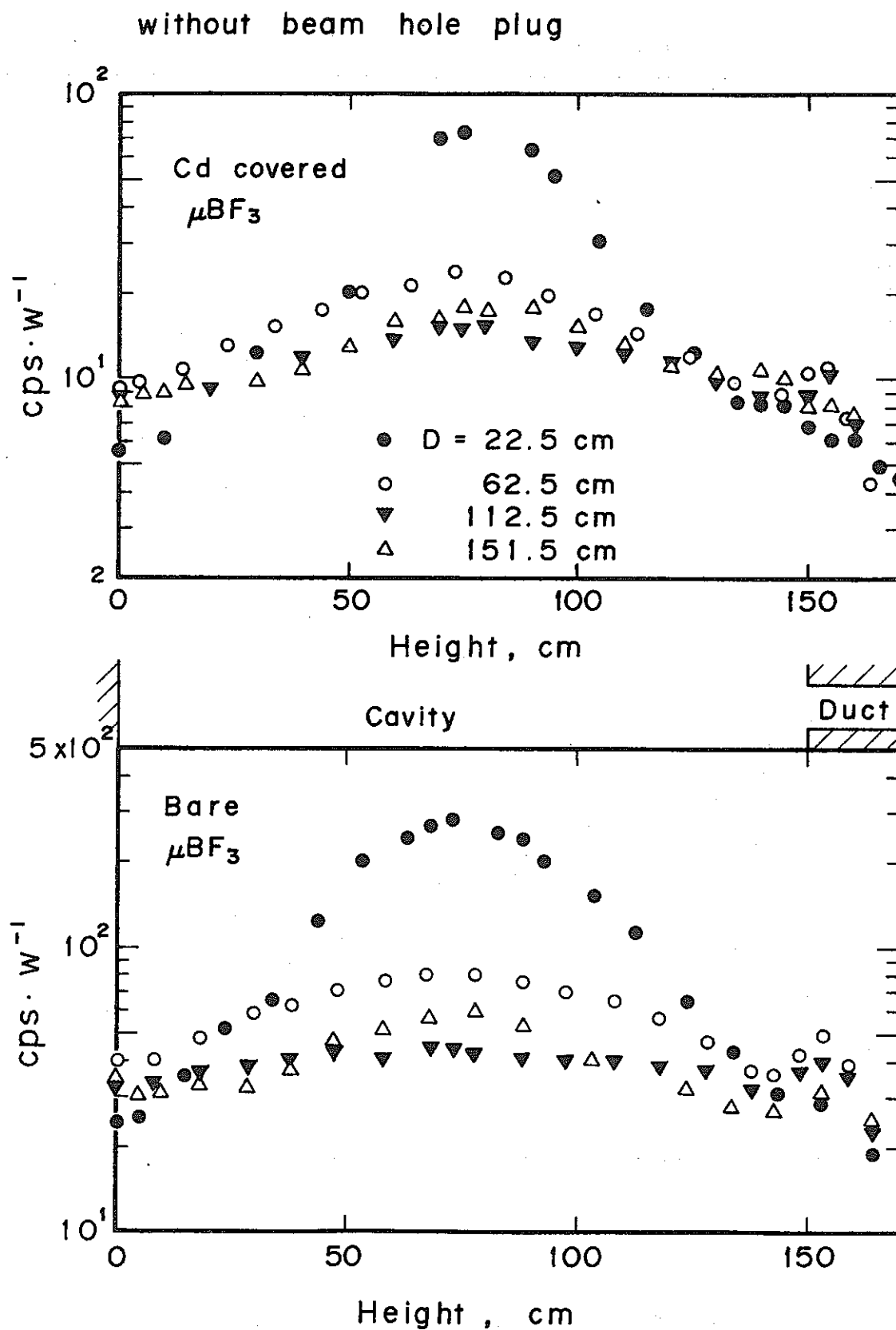


Fig. 4-18 Neutron counting rate distribution in thermal column cavity by  $\mu\text{BF}_3$  counter (Without plug; Upper figure — with Cd cover, Lower figure — without cover)

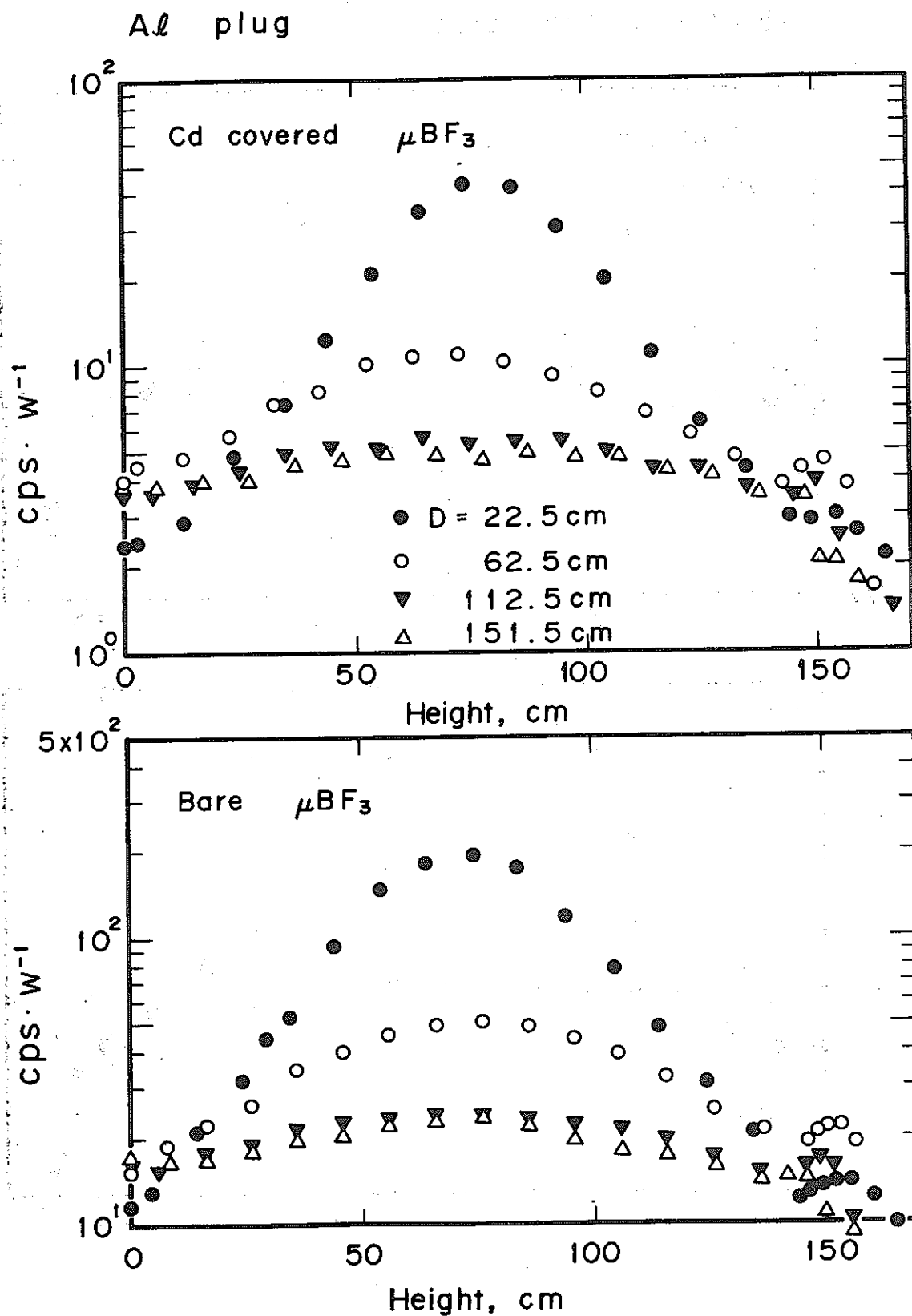


Fig. 4-19 Neutron counting rate distribution in thermal column cavity by  $\mu\text{BF}_3$  counter (Al plug; Upper figure — with Cd cover, Lower figure — without cover)

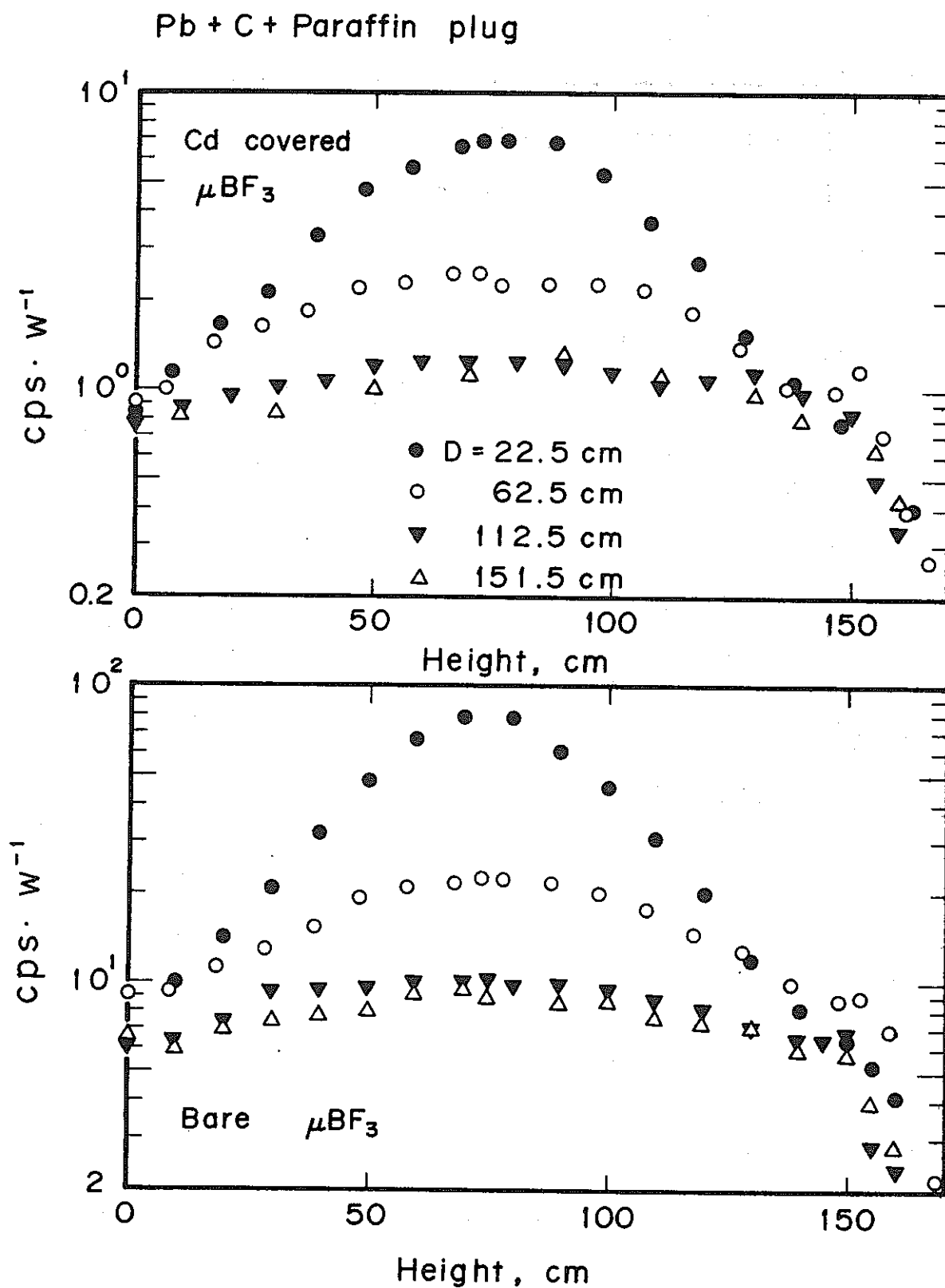
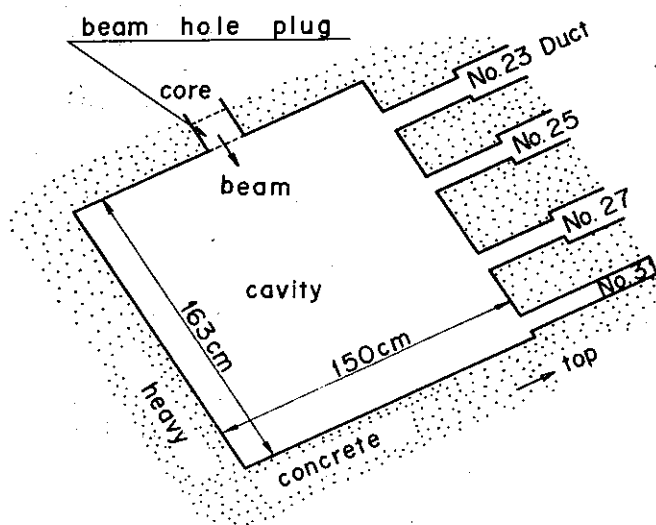
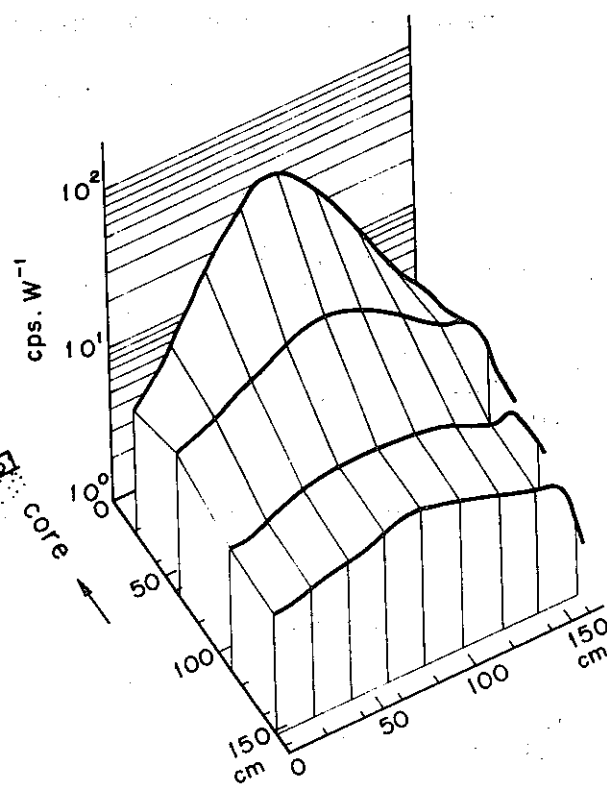


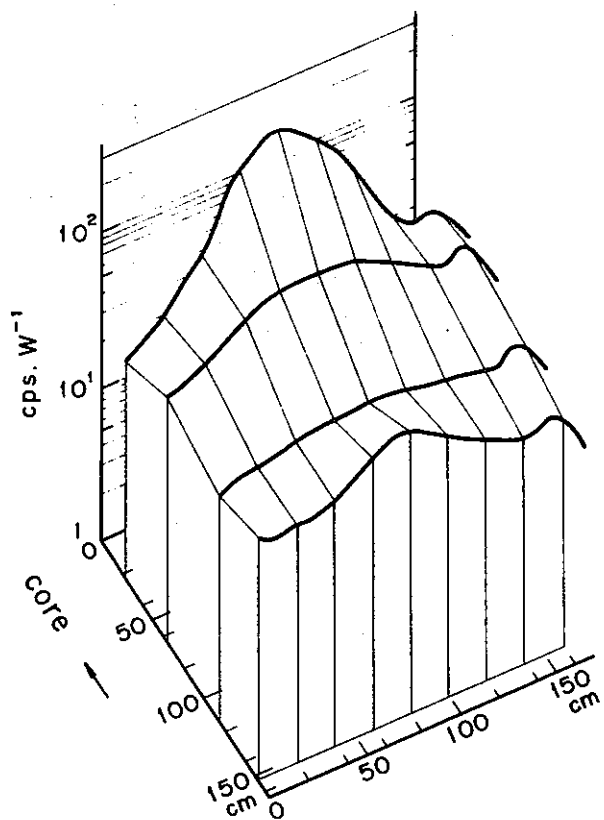
Fig. 4-20 Neutron counting rate distribution in thermal column cavity by  $\mu\text{BF}_3$  counter (Paraffin-contained plug; Upper figure — with Cd cover, Lower figure — without cover)



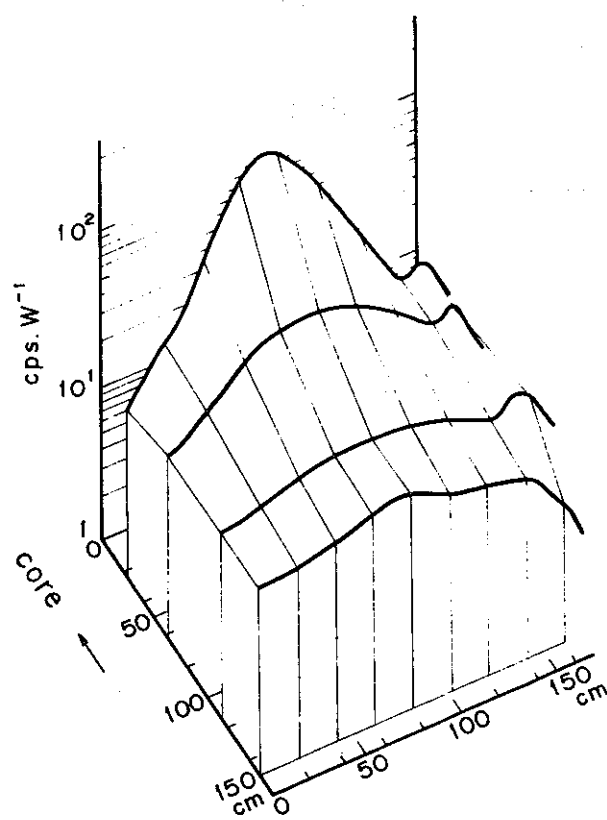
(a) Schematic vertical section of the cavity



(c) Pb+C+Paraffin plug



(b) without beam hole plug



(d) Al beam hole plug

Fig. 4-21 Neutron counting rate distribution in thermal column cavity by  $\mu\text{BF}_3$  counter

Table 4.1 Reaction rate distributions and cadmium ratios in the cavities by gold foils and indium foils

cavity	beam hole plug	foil position	cadmium ratio of $^{197}\text{Au}(n,\gamma)$	reaction rate $\text{sec}^{-1}$ at 2kw	
				$^{197}\text{Au}(n,\gamma)$ bare	$^{115}\text{In}(n,n')$
thermal column	none	A*	1.4	$4.0 \times 10^{-14}$	$4.7 \times 10^{-17}$
		B	1.3	$8.2 \times 10^{-16}$	
	Pb+C+paraffin	A	9.2	$2.4 \times 10^{-15}$	$5.8 \times 10^{-19}$
		B	1.9	$1.1 \times 10^{-16}$	
	aluminum	A	1.4	$2.1 \times 10^{-14}$	$4.2 \times 10^{-18}$
		B	1.5	$4.1 \times 10^{-16}$	
fast column	none	A	1.3	$3.6 \times 10^{-14}$	$2.7 \times 10^{-17}$
		C	1.4	$1.2 \times 10^{-15}$	
	Pb+C+paraffin	A	8.6	$1.8 \times 10^{-15}$	$3.3 \times 10^{-19}$
		C	1.7	$1.3 \times 10^{-16}$	
	aluminum	A	1.3	$2.4 \times 10^{-14}$	$2.1 \times 10^{-18}$
		C	1.6	$5.2 \times 10^{-16}$	

\*A: surface of beam hole plug

B: entrance of No.25 duct

C: entrance of No.26 duct

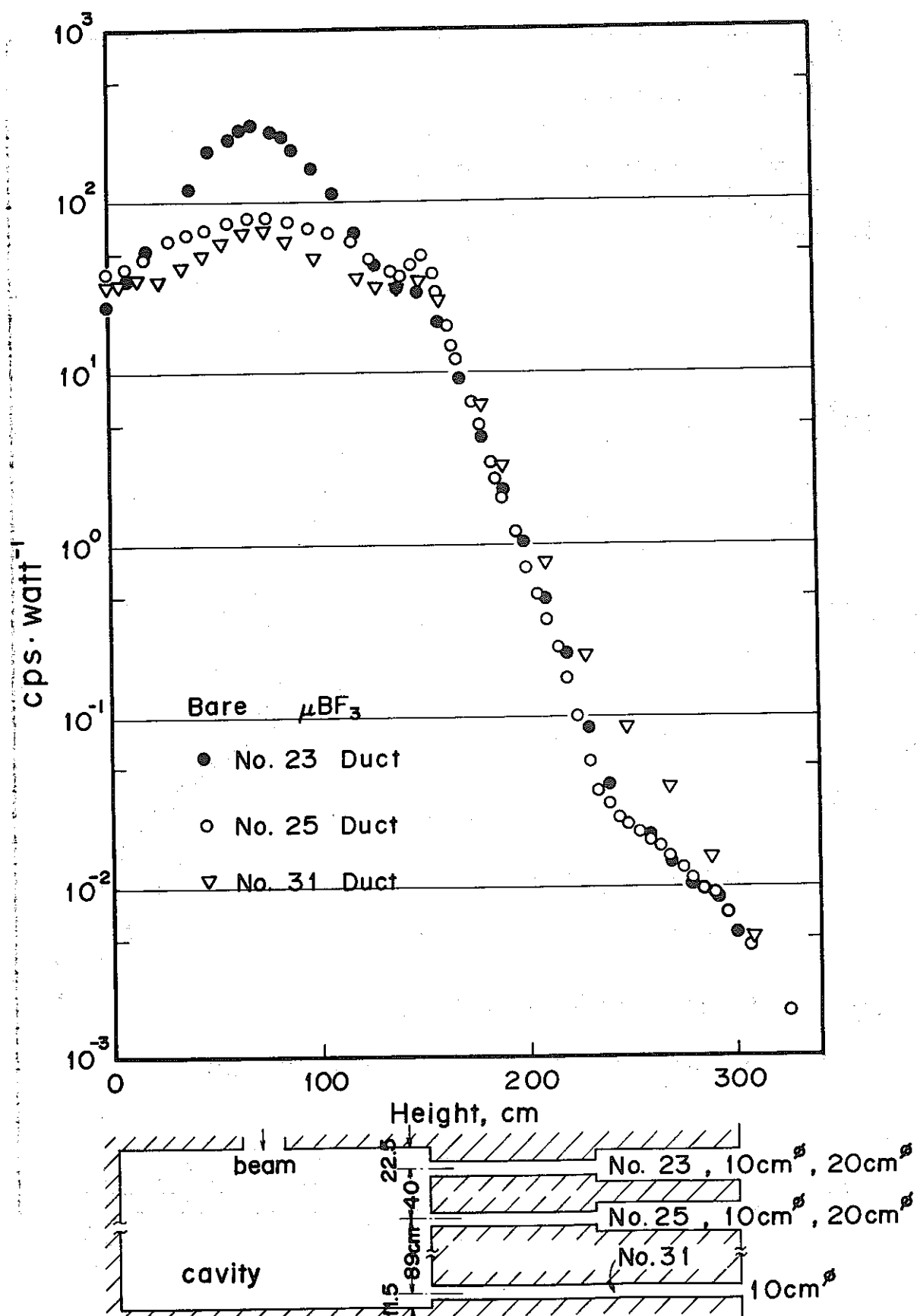


Fig. 4-22 Neutron counting rate (Without plug) on ducts axes of No. 23, No. 25, No. 31 by  $\mu\text{BF}_3$  counter (bare)

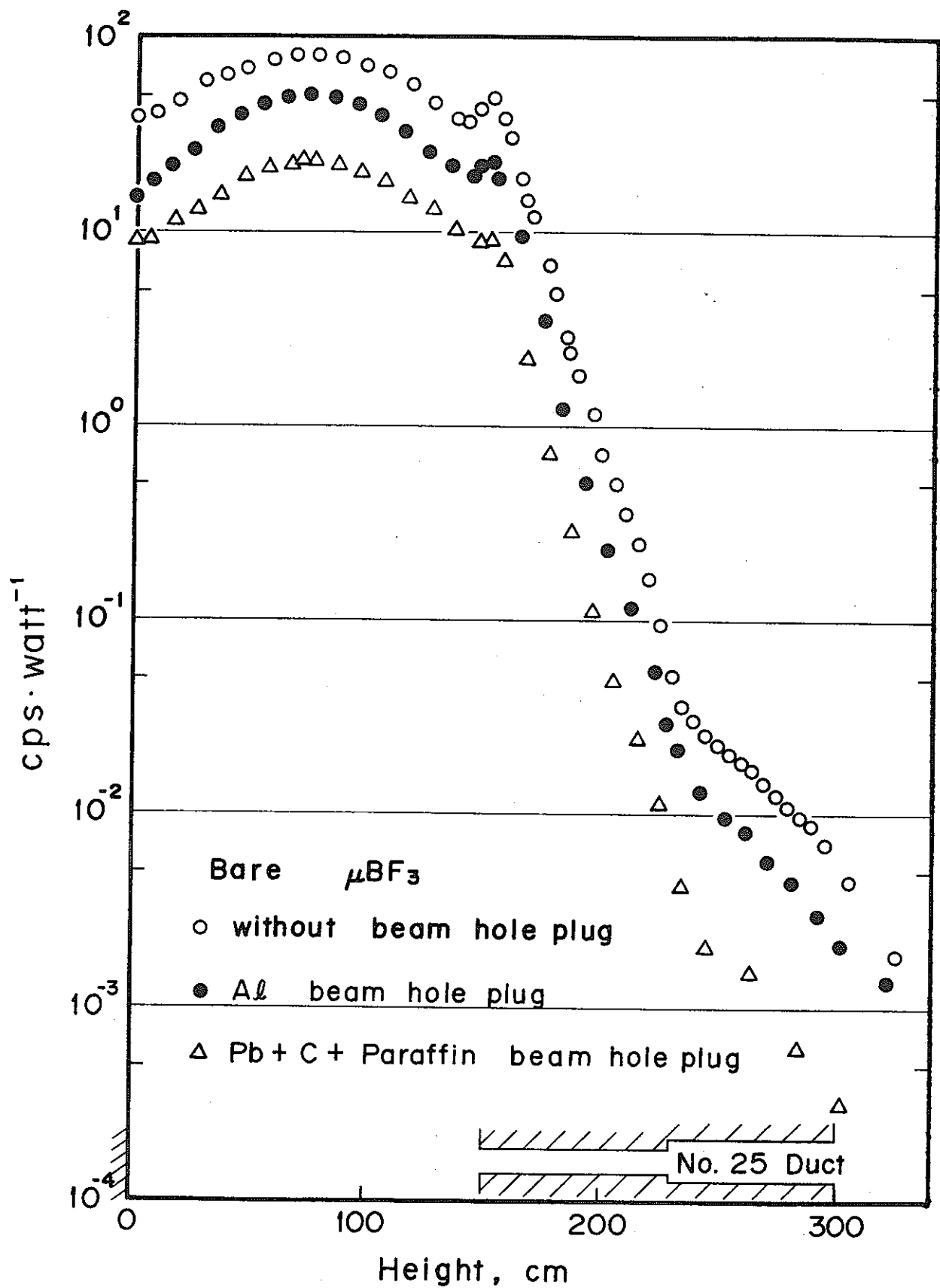


Fig. 4-23 Neutron counting rate on No. 25 duct axis by  $\mu\text{BF}_3$  counter (bare) — "Without plug", "Al plug", "Paraffin-contained plug"

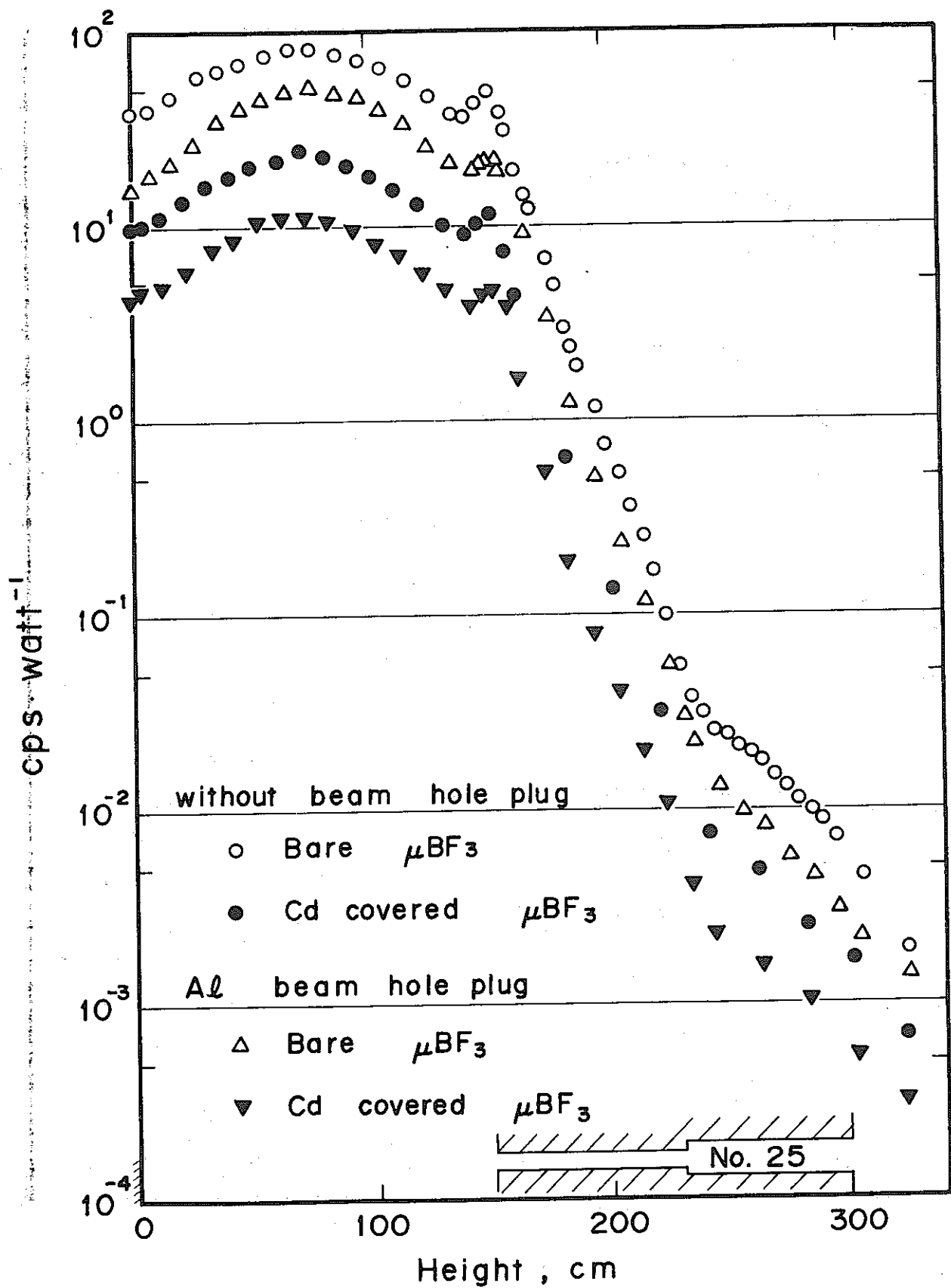


Fig. 4-24 Neutron counting rate of  $\mu\text{BF}_3$  counter on No. 25 duct axis — "Without plug", "Al plug"

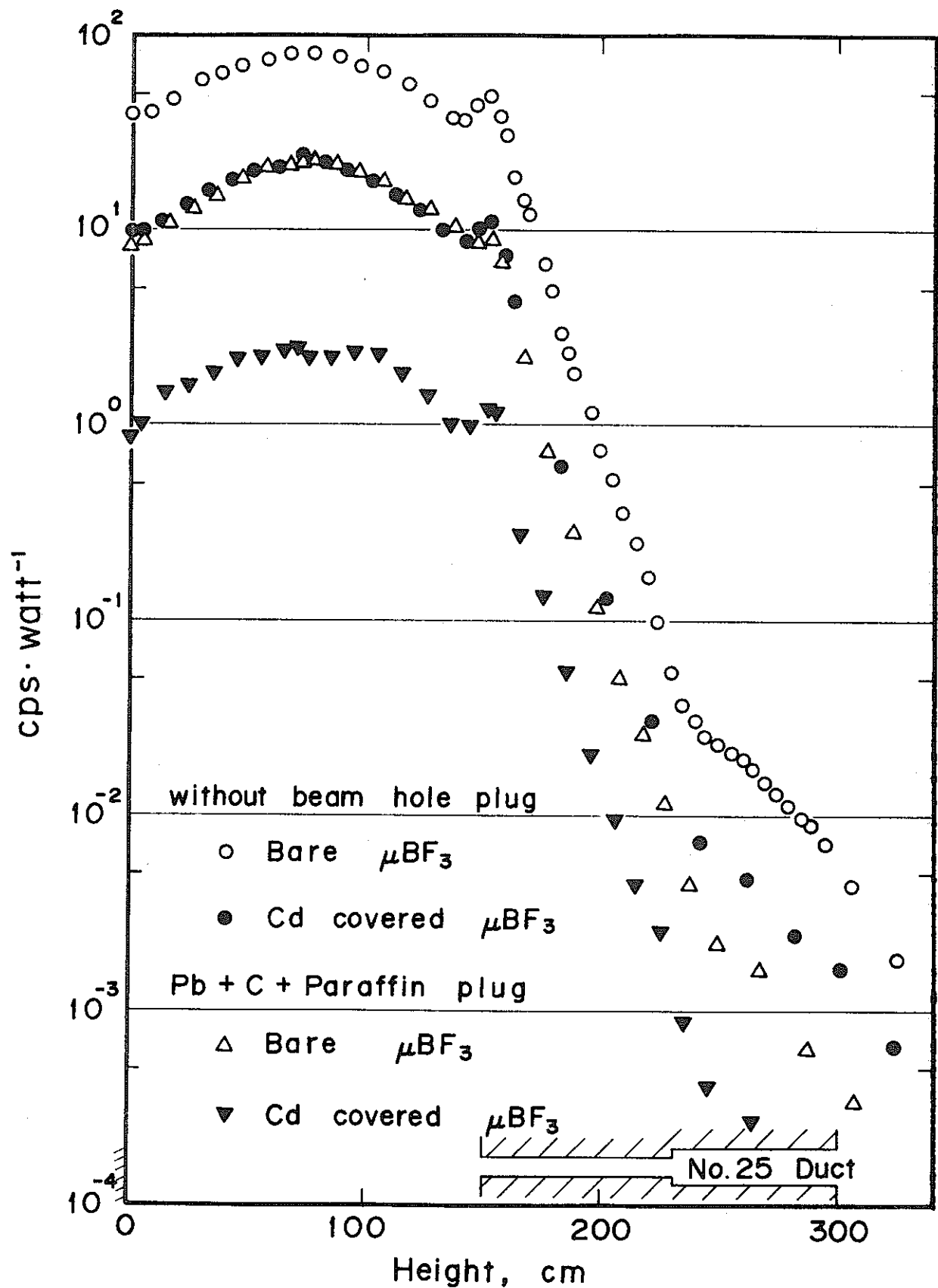


Fig. 4-25 Neutron counting rate of  $\mu\text{BF}_3$  counter on No. 25 duct axis — "Without plug", "Paraffin-contained plug"

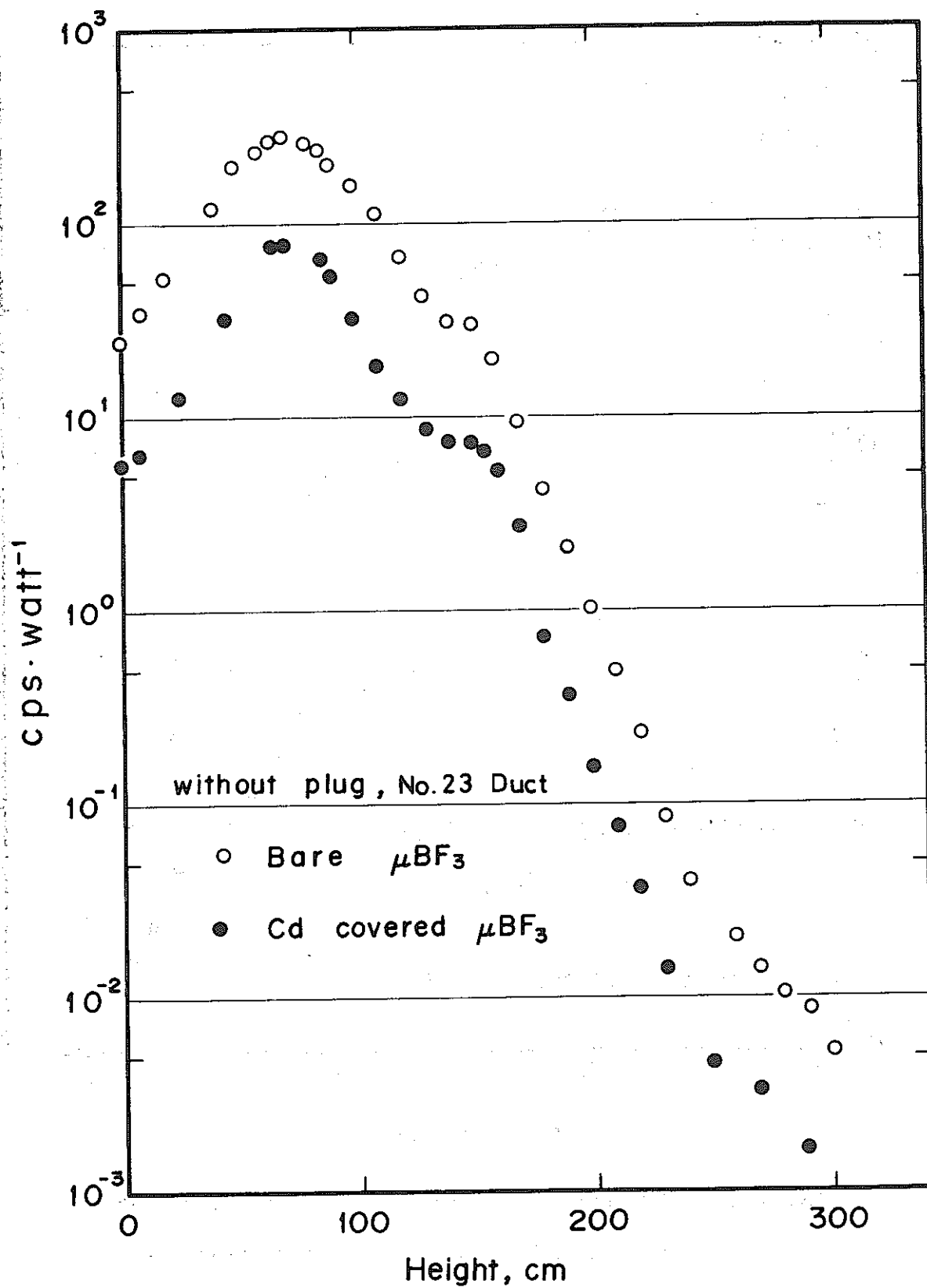


Fig. 4-26 Neutron counting rate distribution of  $\mu\text{BF}_3$  counter on No. 23 duct — "Without plug"

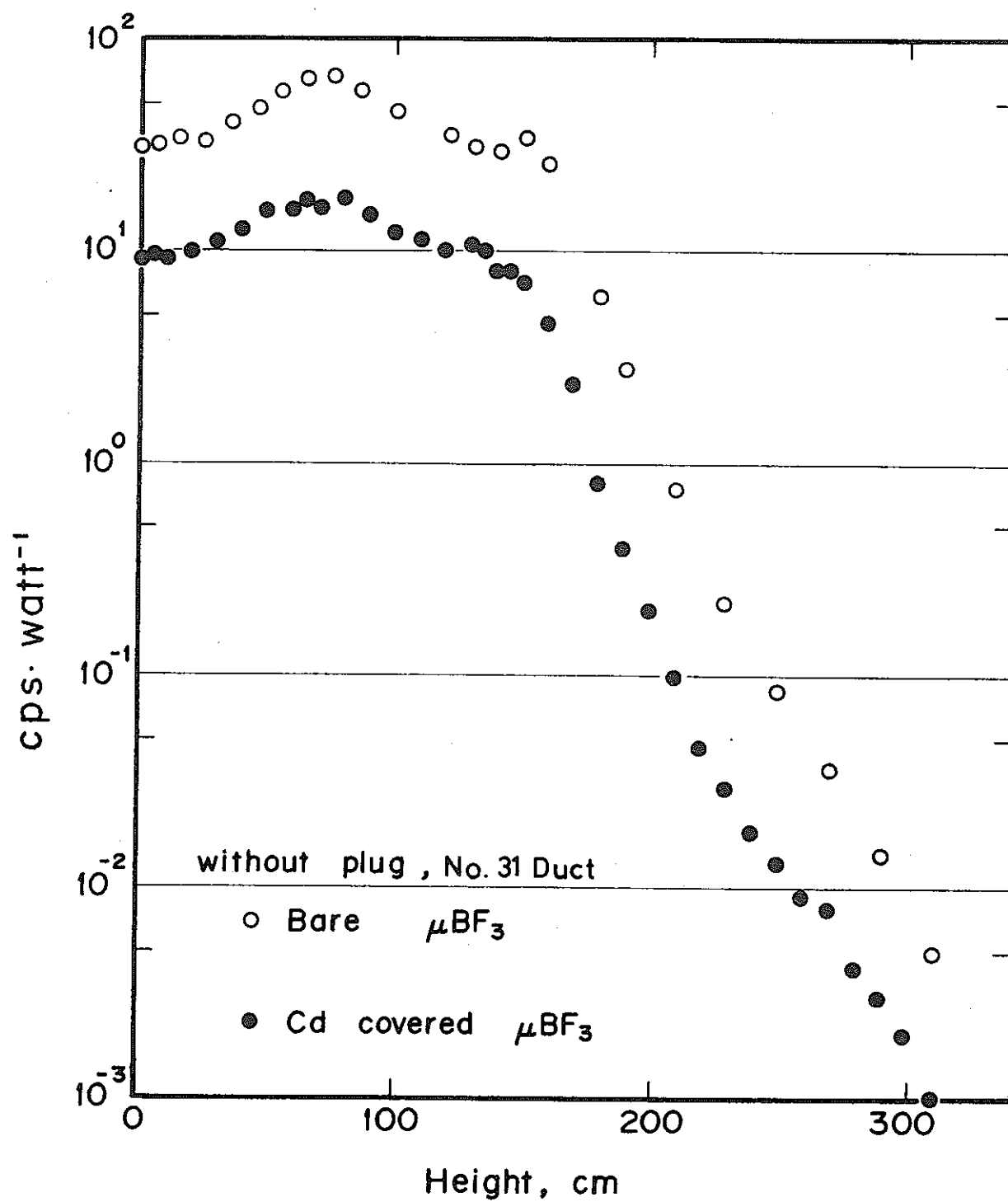


Fig. 4-27 Neutron counting rate distribution of  $\mu\text{BF}_3$  counter on No. 31 duct axis —  
"Without plug"

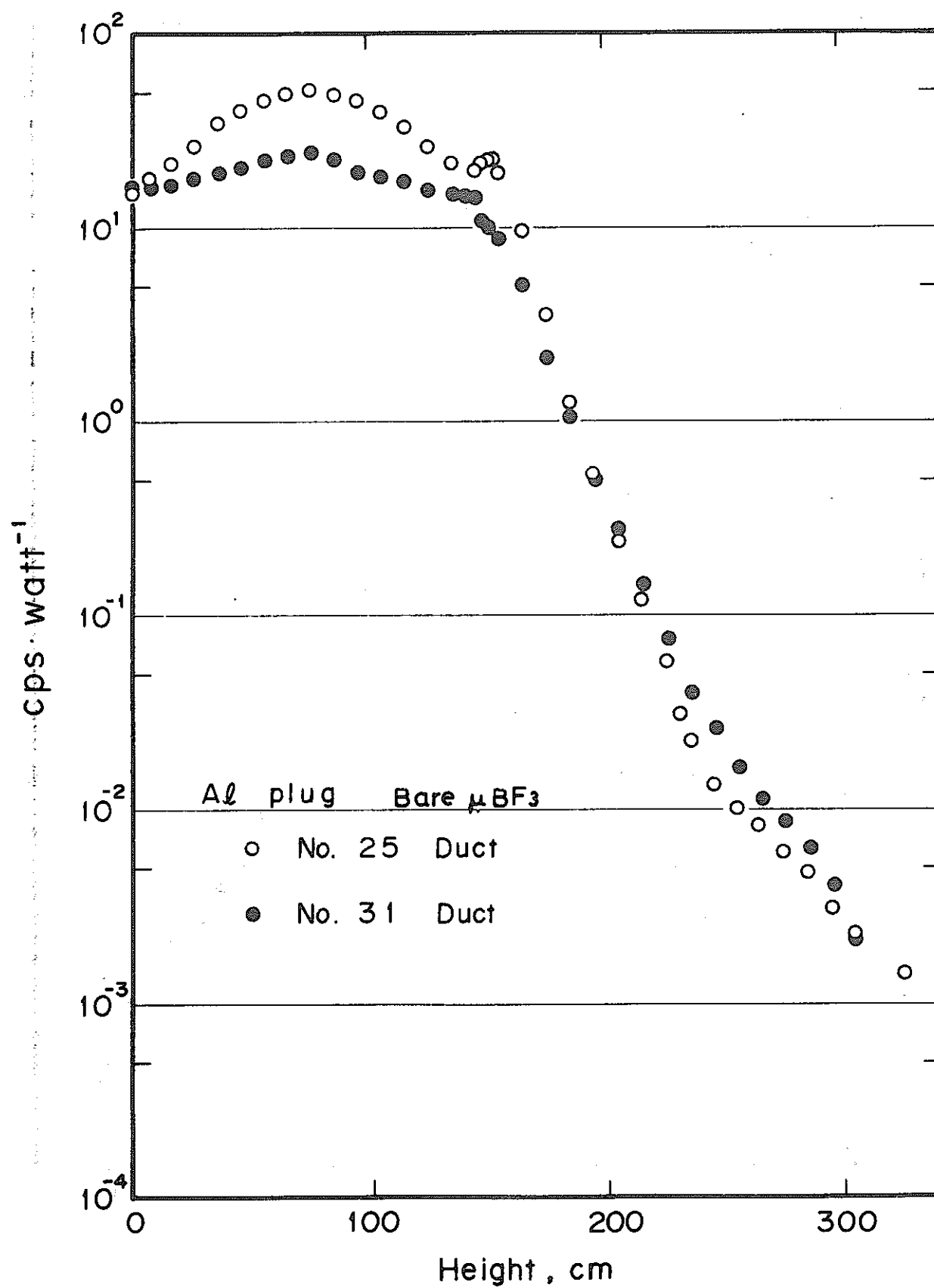


Fig. 4-28 Neutron counting rate on duct axes of No. 25, No. 31 by  $\mu\text{BF}_3$  counter — "Al plug"

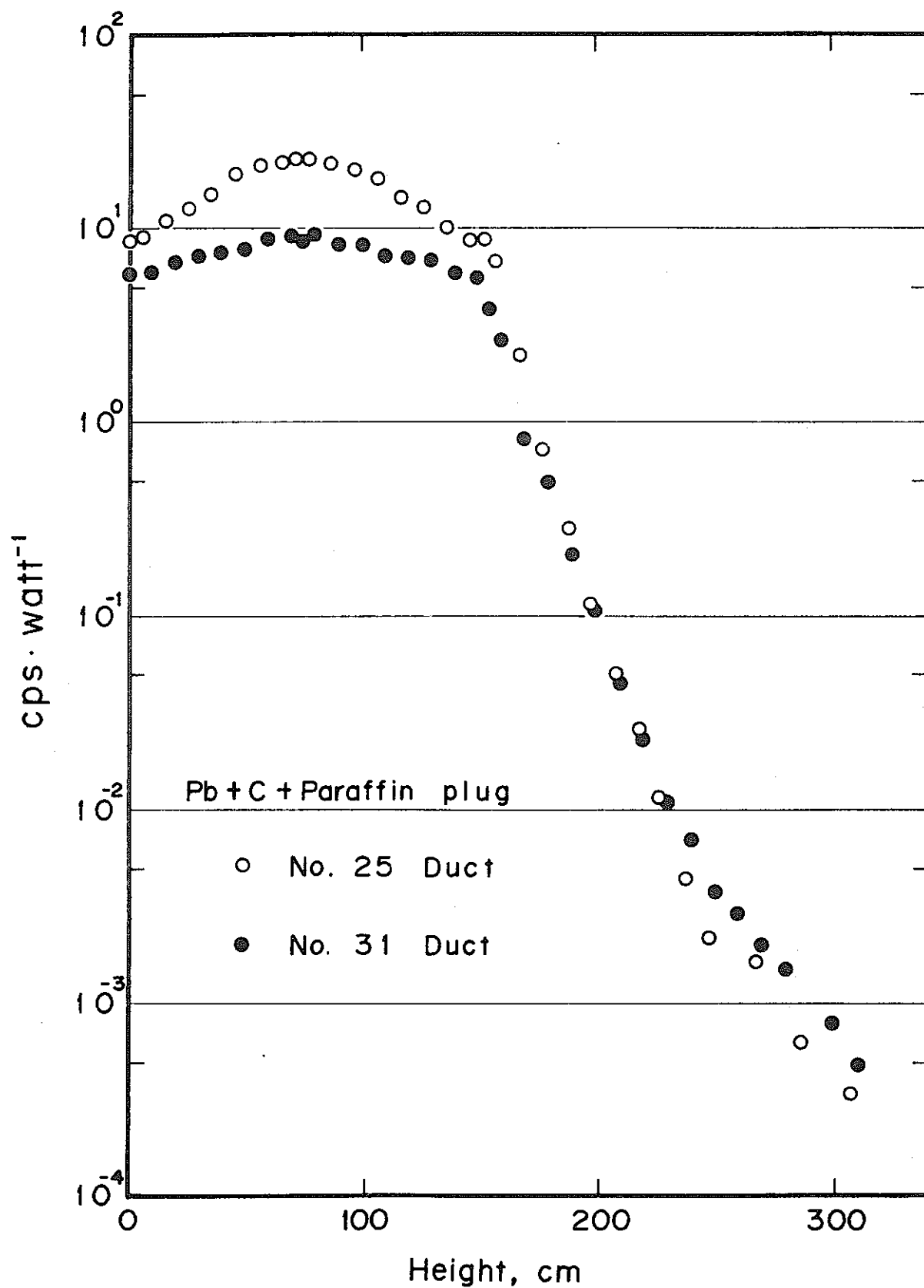


Fig. 4-29 Neutron counting rate on duct axes of No. 25, No. 31 by  $\mu\text{BF}_3$  counter — "Paraffin-coated plug"

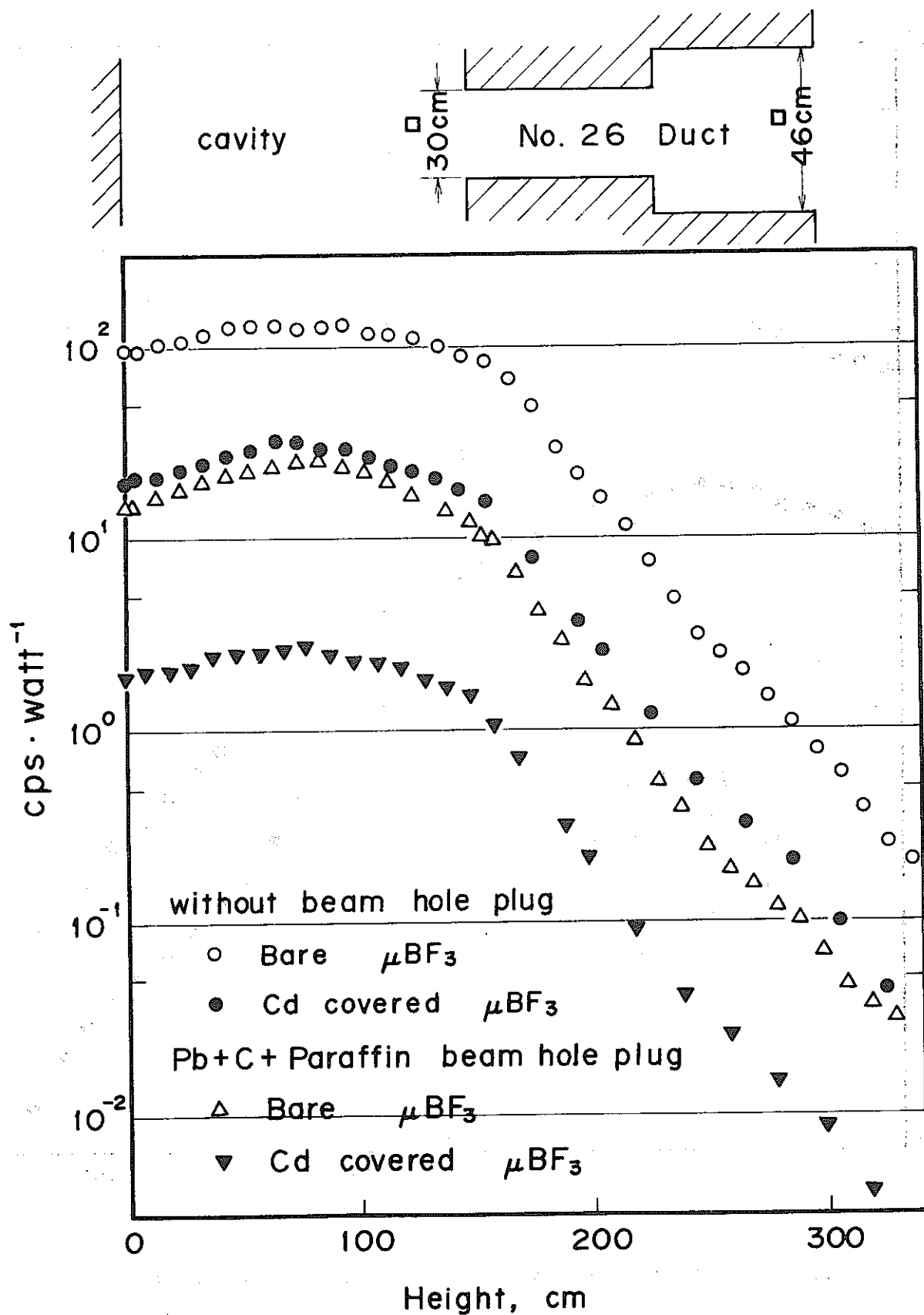


Fig. 4-30 Neutron counting rate on No. 26 duct axis by  $\mu\text{BF}_3$  counter — "Without plug", "Paraffin-contained plug"

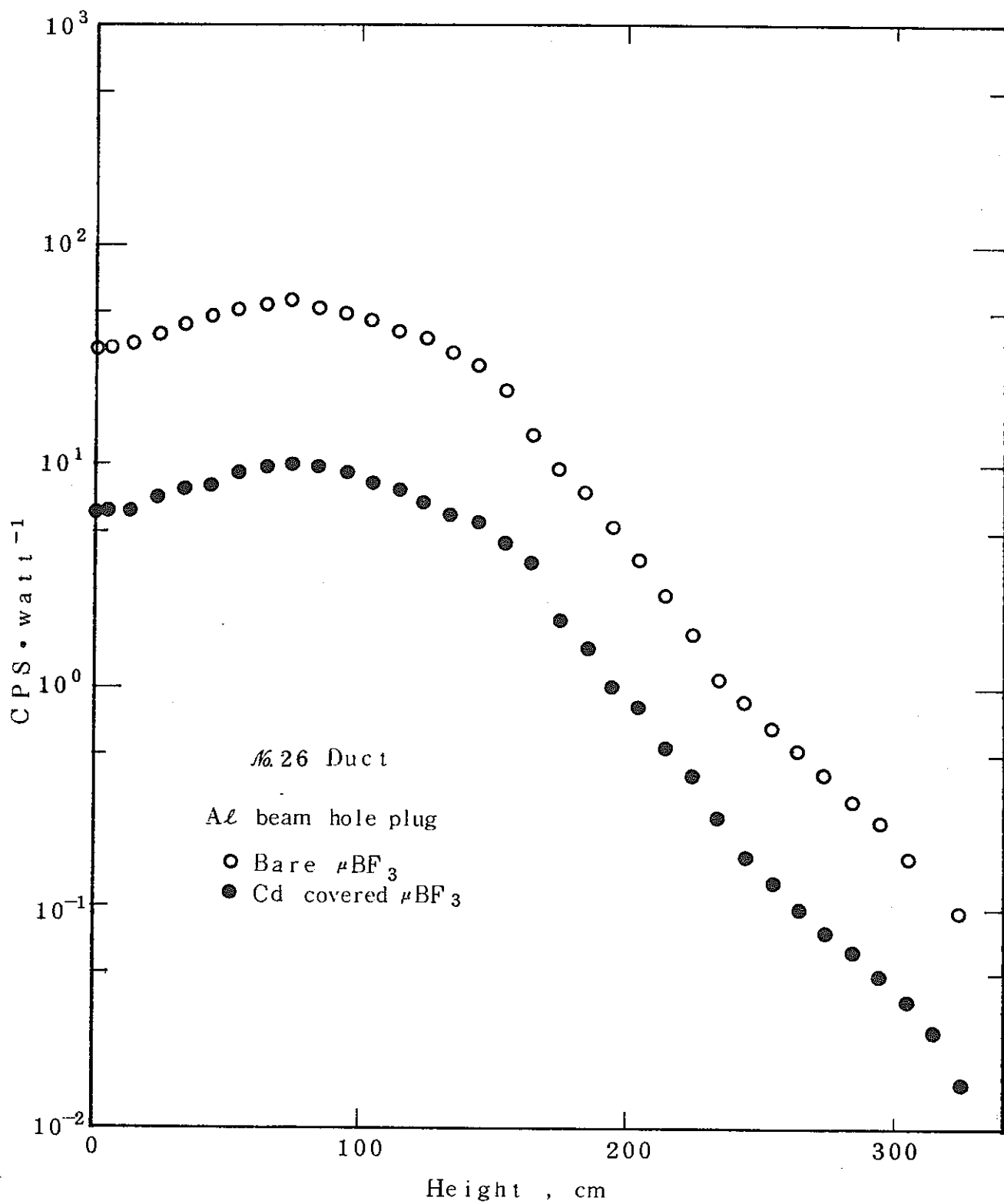


Fig. 4-31 Neutron counting rate on No. 26 duct axis  
 — "Al plug"

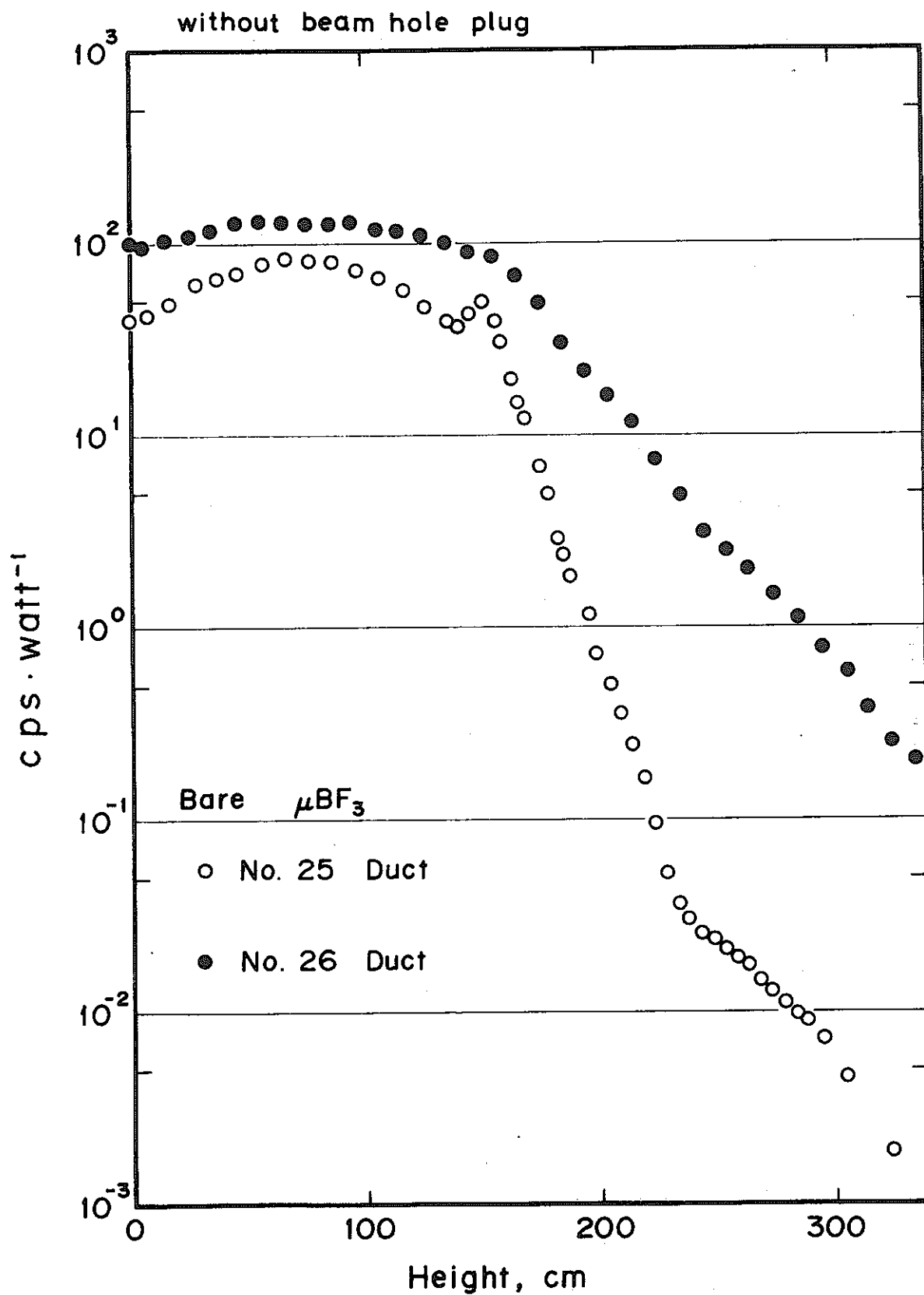


Fig. 4-32 Neutron counting rate on duct axes of No. 25, No. 26 by  $\mu\text{BF}_3$  counter — "Without plug"

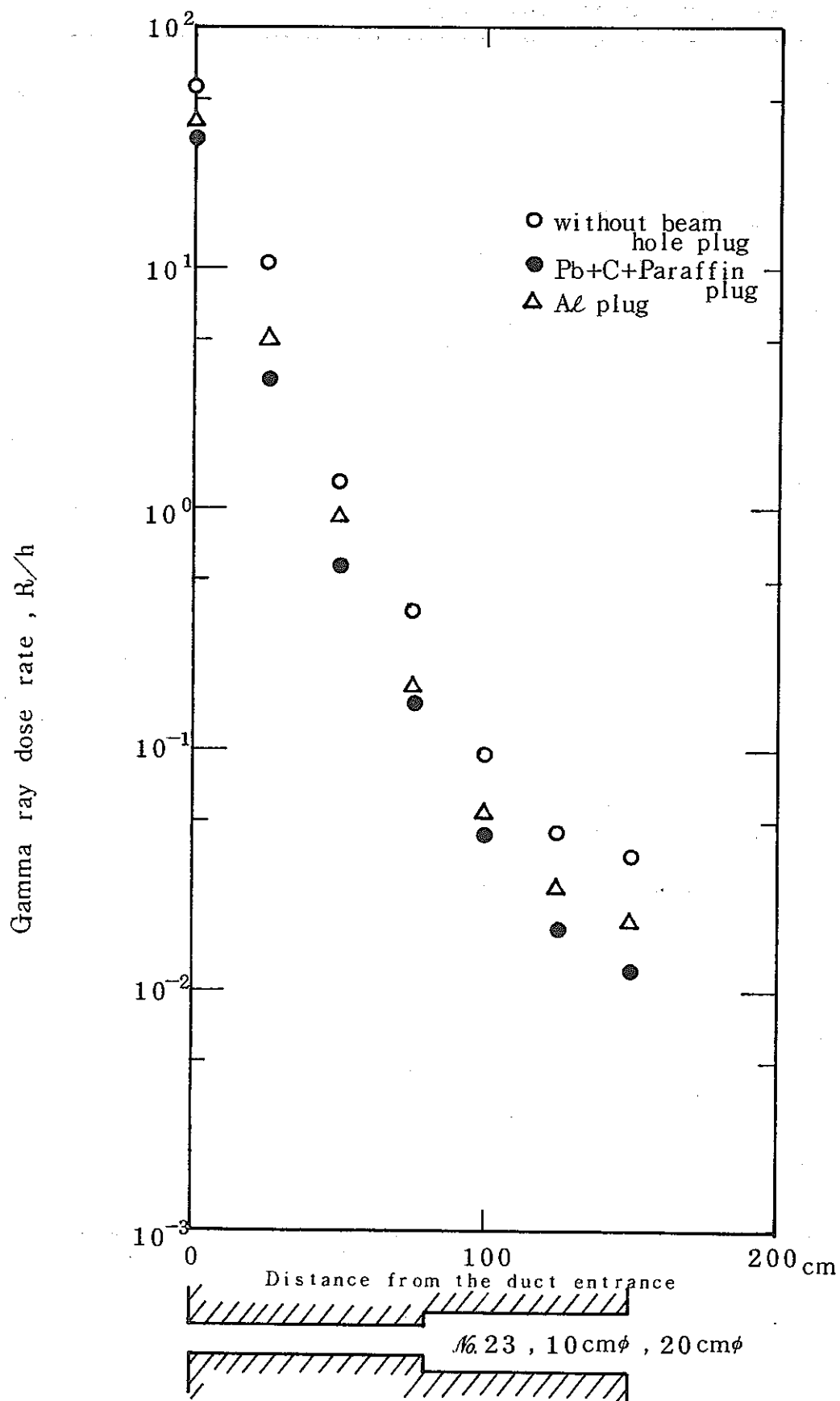


Fig. 4-33 Gamma-ray dose rate in No. 23 duct by TLD — "Without plug", "Al plug", "Paraffin-contained plug"

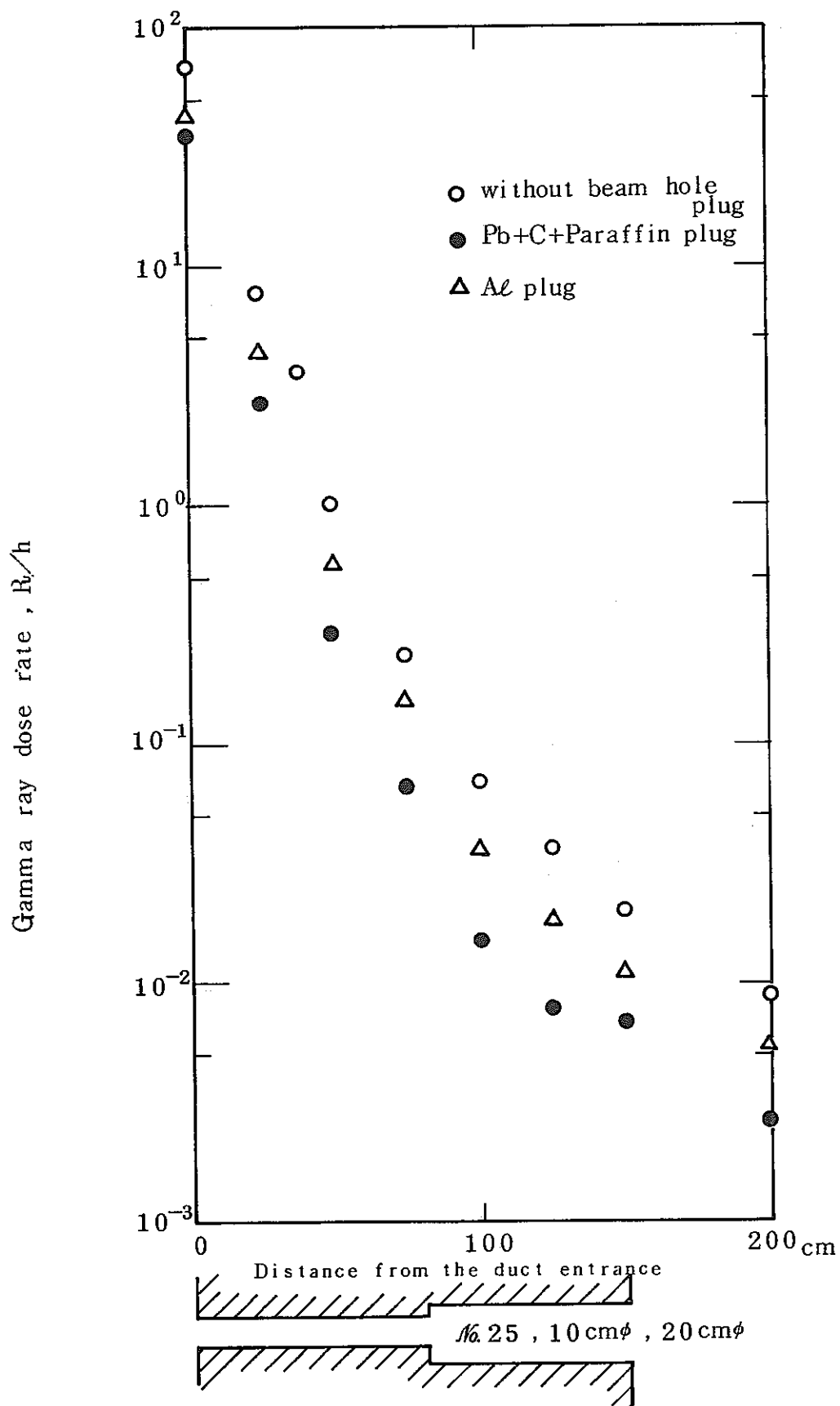


Fig. 4-34 Gamma-ray dose rate in No. 25 duct by TLD — "Without plug", "Al plug", "Paraffin-contained plug"

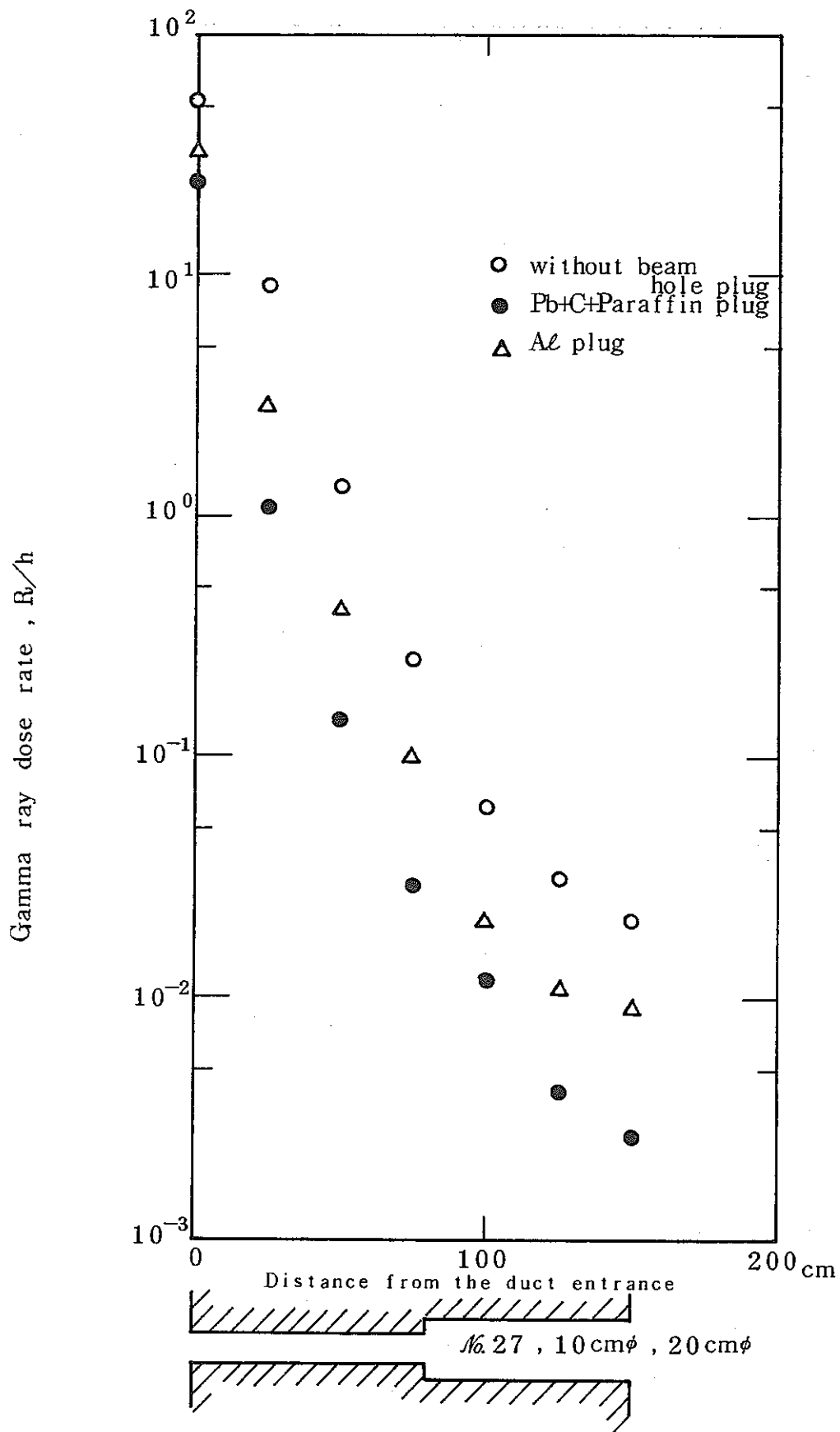


Fig. 4-35 Gamma-ray dose rate in No. 27 duct by TLD — "Without plug", "Al plug", "Paraffin-contained plug"

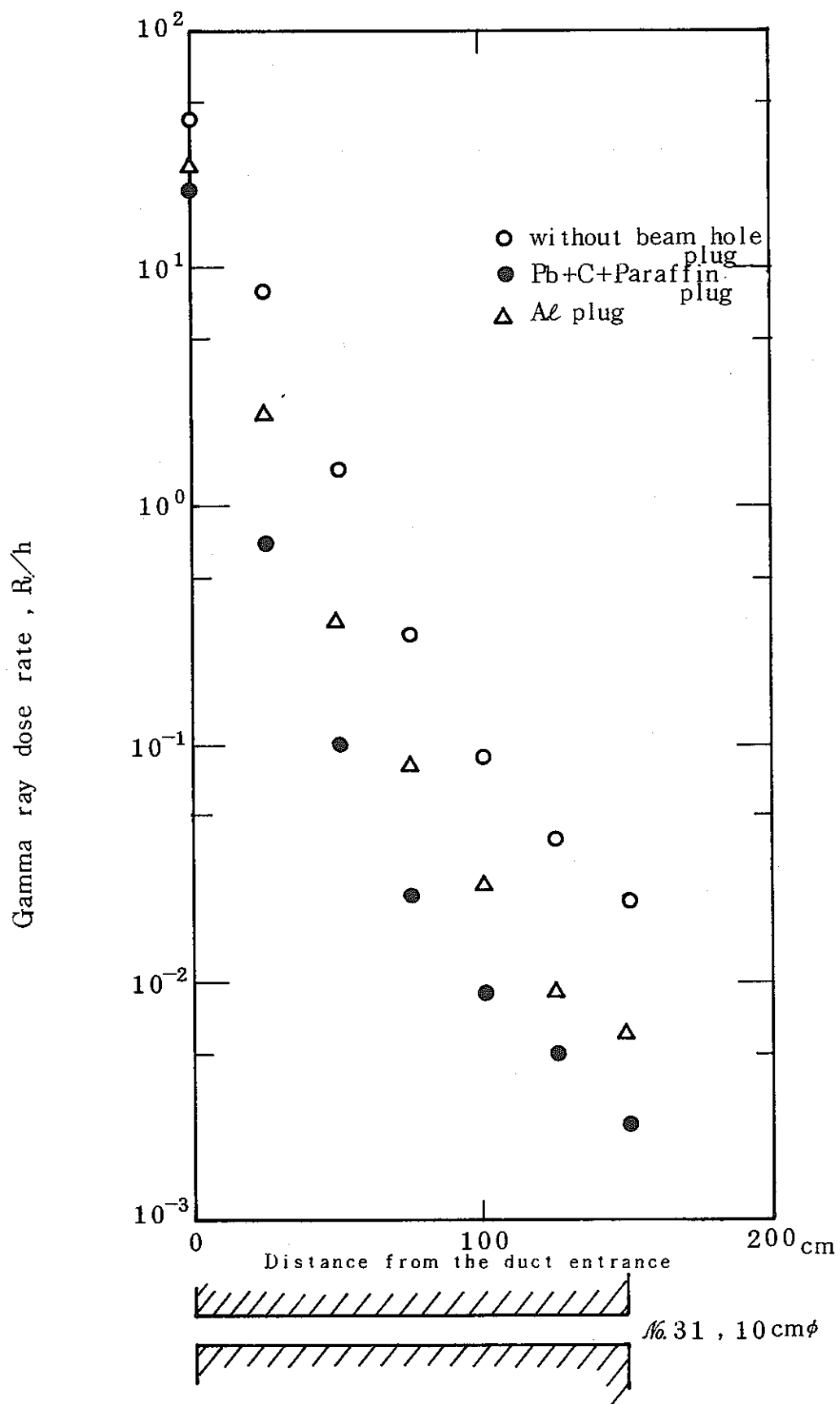


Fig. 4-36 Gamma-ray dose rate in No. 31 duct by TLD — "Without plug", "Al plug", "Paraffin-contained plug"

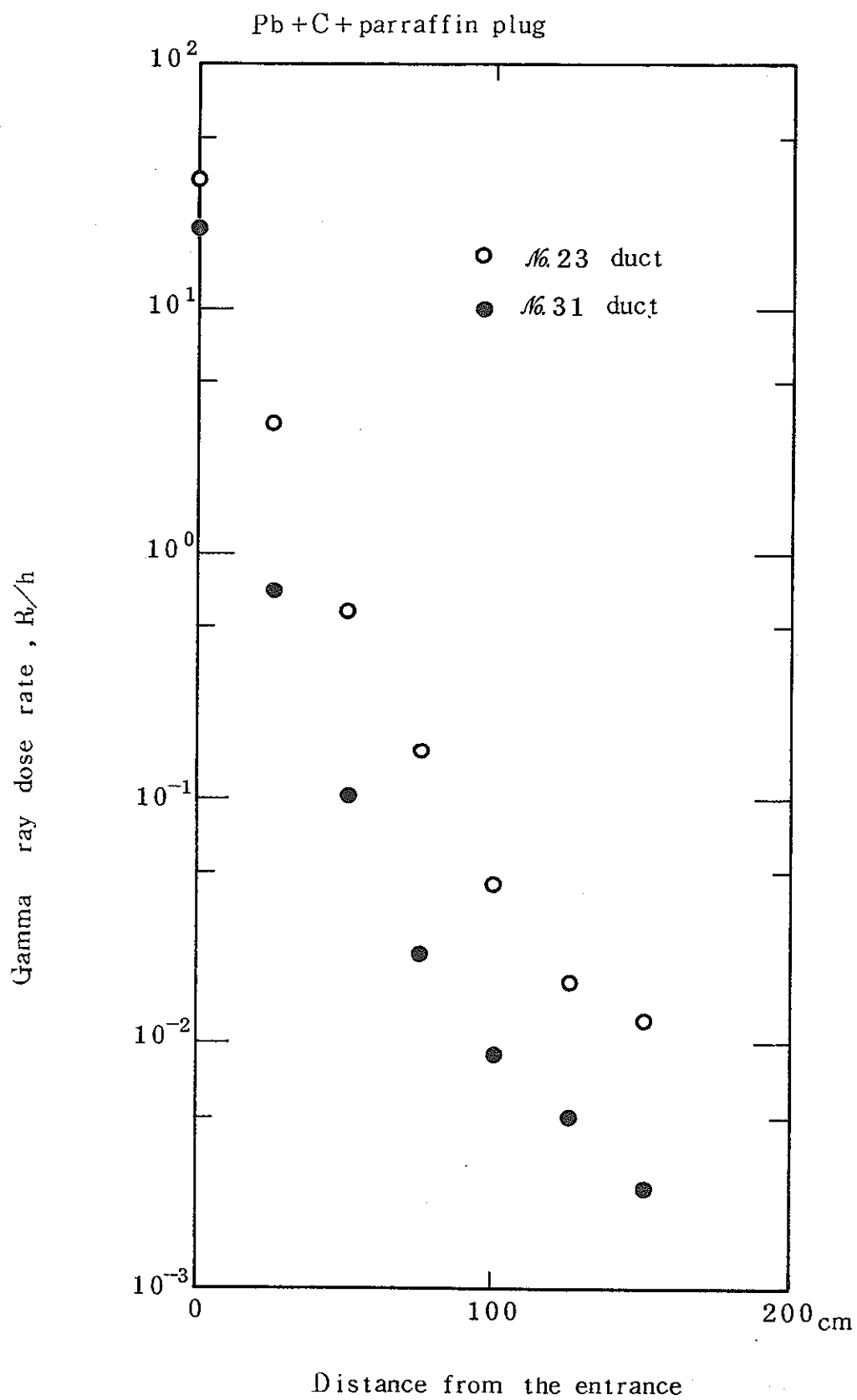


Fig. 4-37 Gamma-ray dose rate in ducts of No. 23,  
No. 31 by TLD — "Paraffin-contained plug"

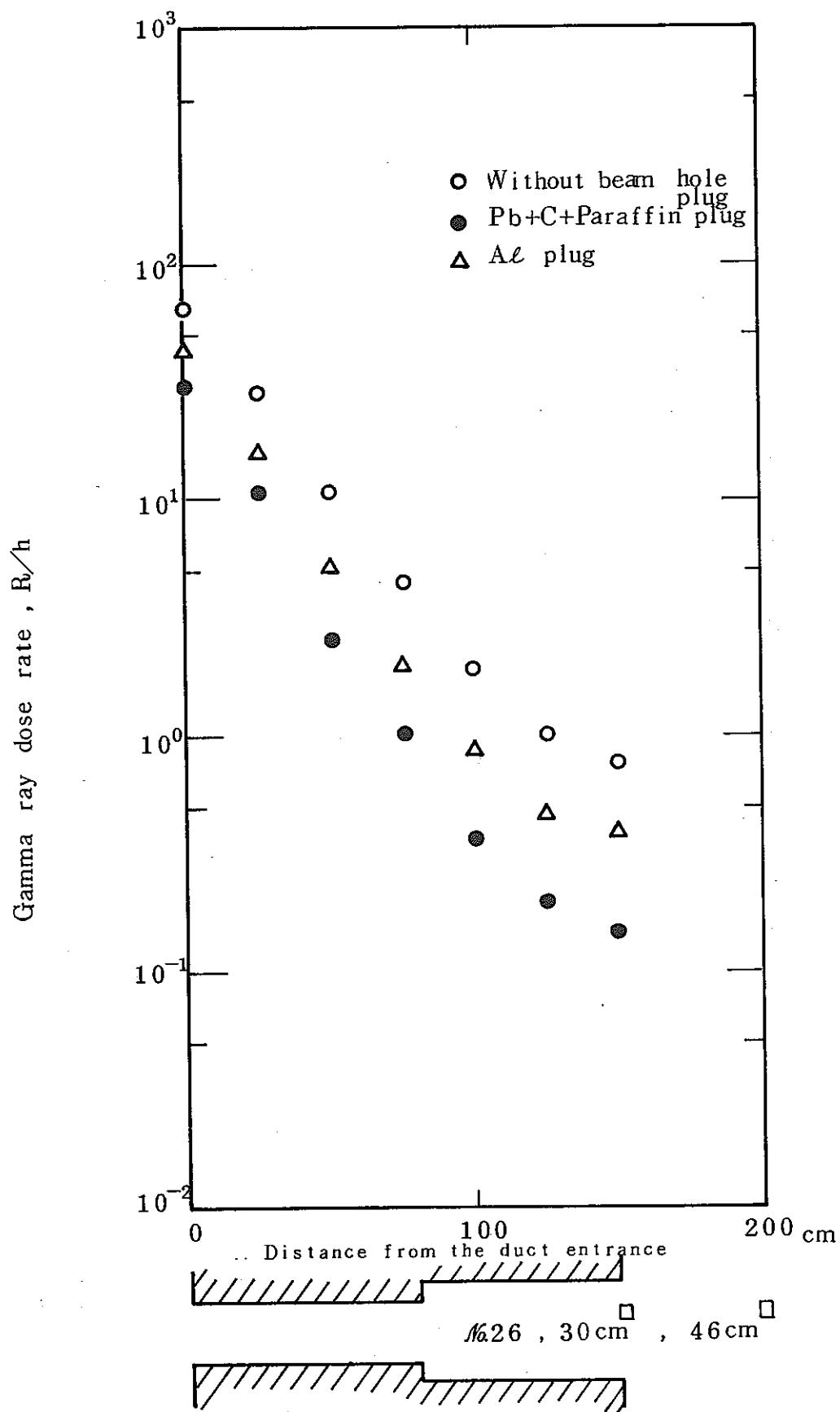


Fig. 4-38 Gamma-ray dose rate in No. 26 duct by TLD — "Without plug", "Al plug", "Paraffin-contained plug"

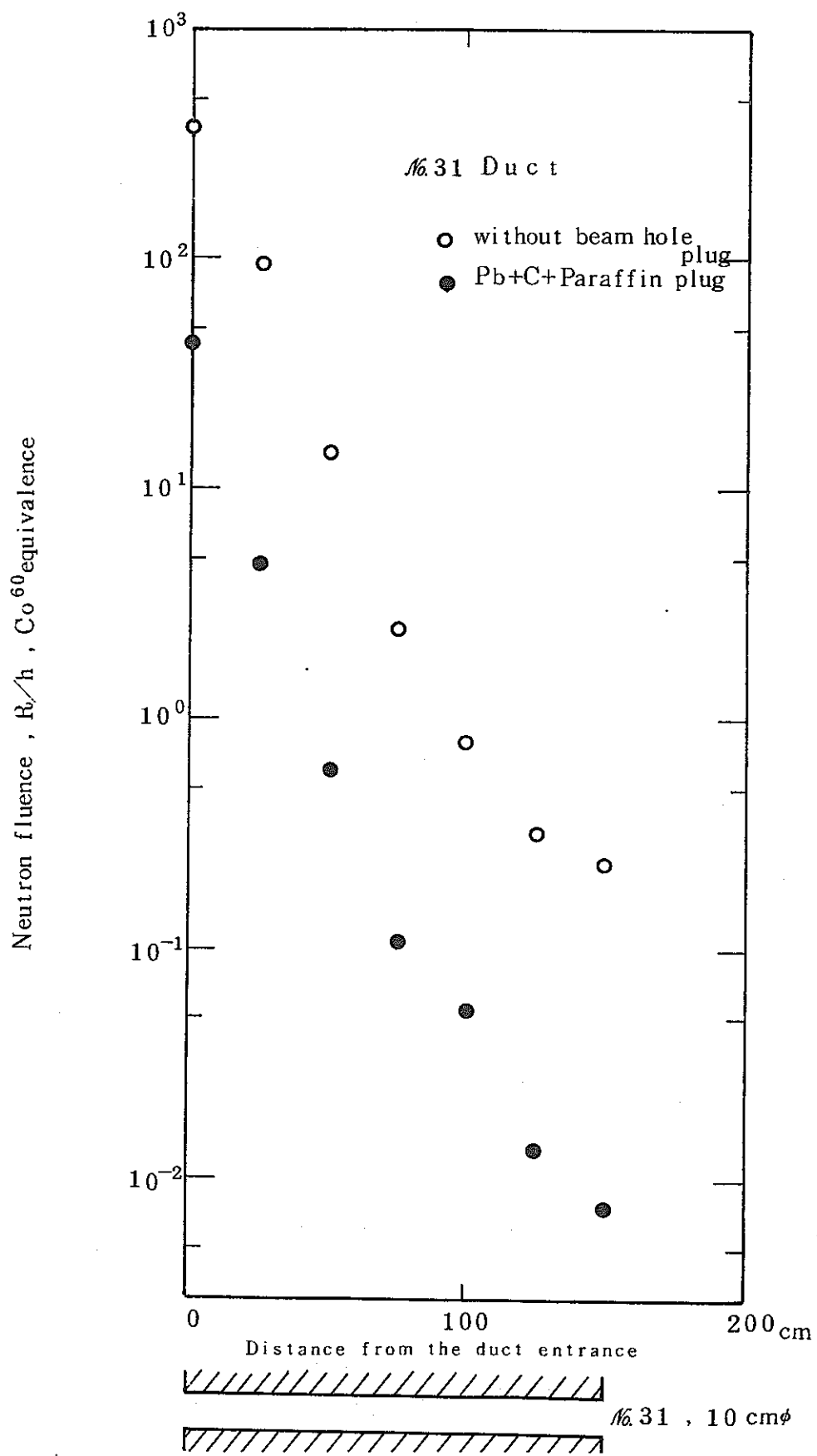


Fig. 4-39 Neutron reaction rate in No. 31 duct by  $^6LiF$  TLD — "Without plug", "Paraffin-contained plug"

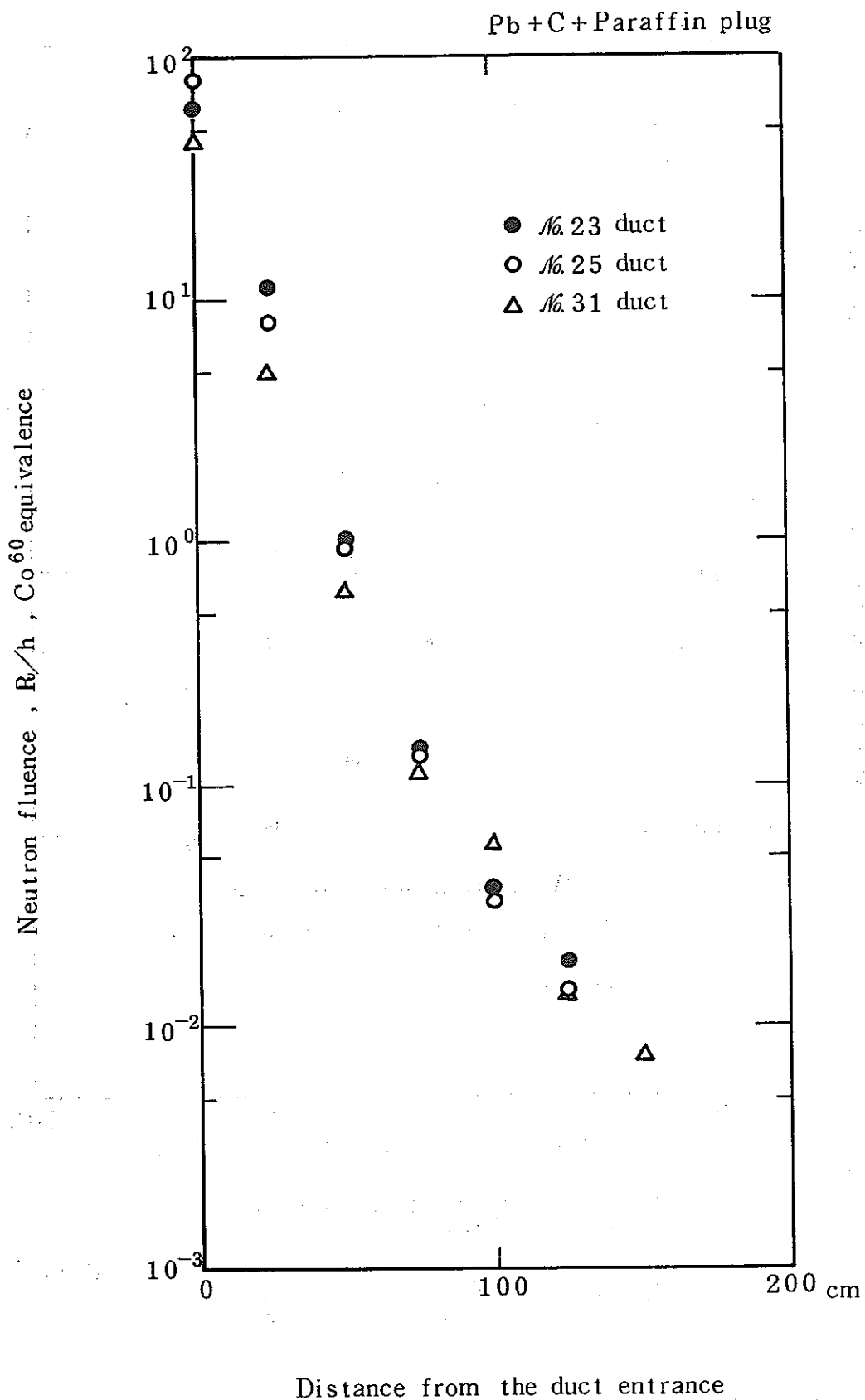


Fig. 4-40 Neutron reaction rate in ducts of No. 23, No. 25, No. 31 by  $^6LiF$  TLD — "Paraffin-contained plug"

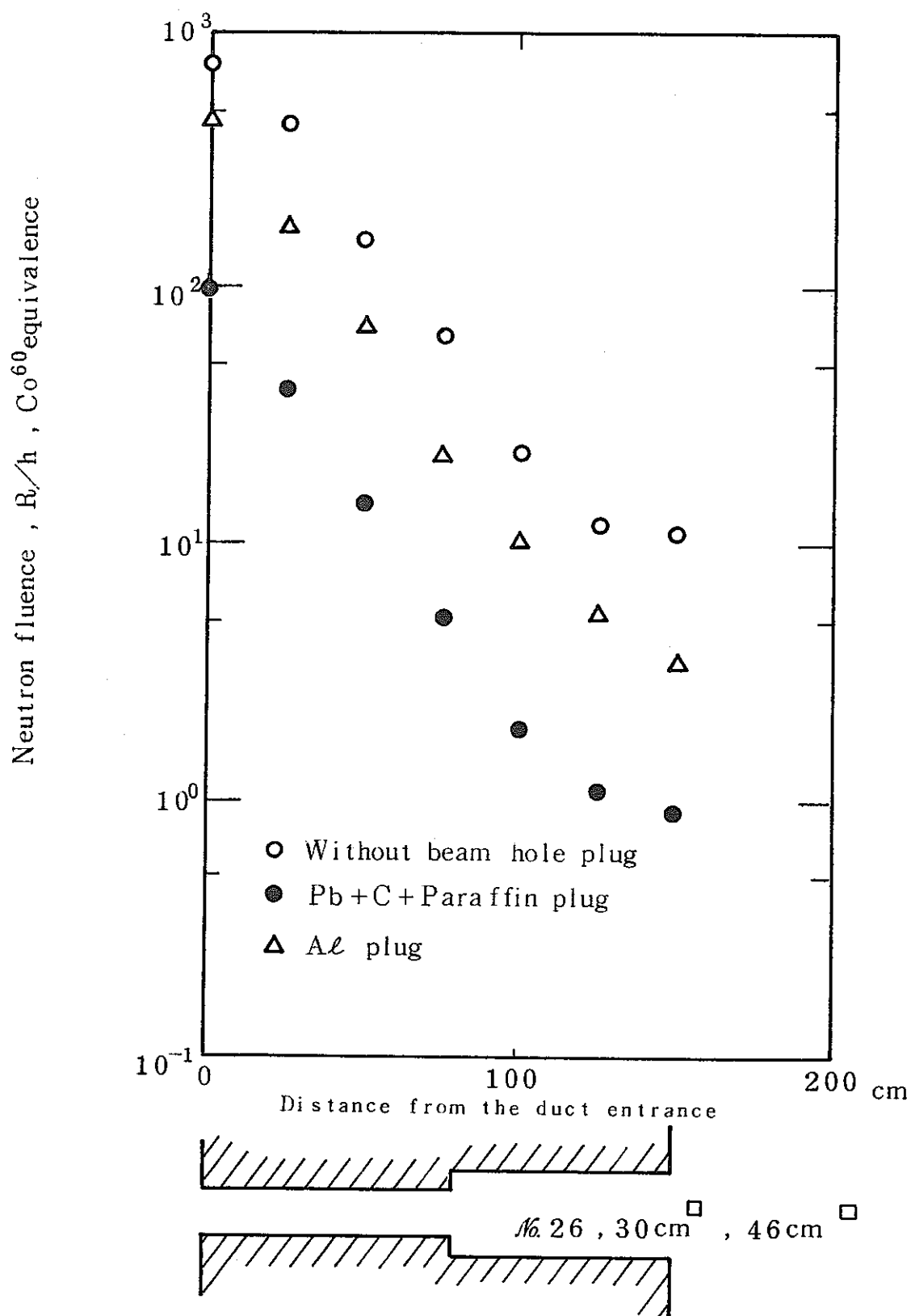


Fig. 4-41 Neutron reaction rate in No. 26 duct by  $^6\text{LiF}$  TLD — "Without plug", "Al plug", "Paraffin-contained plug"

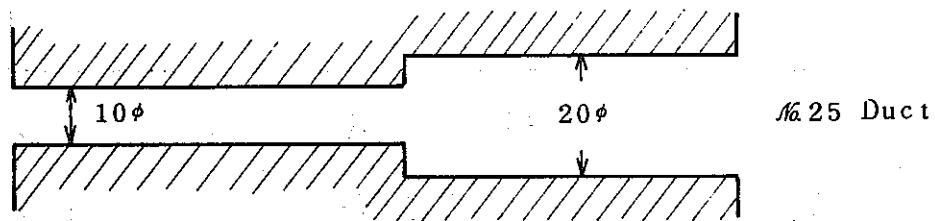
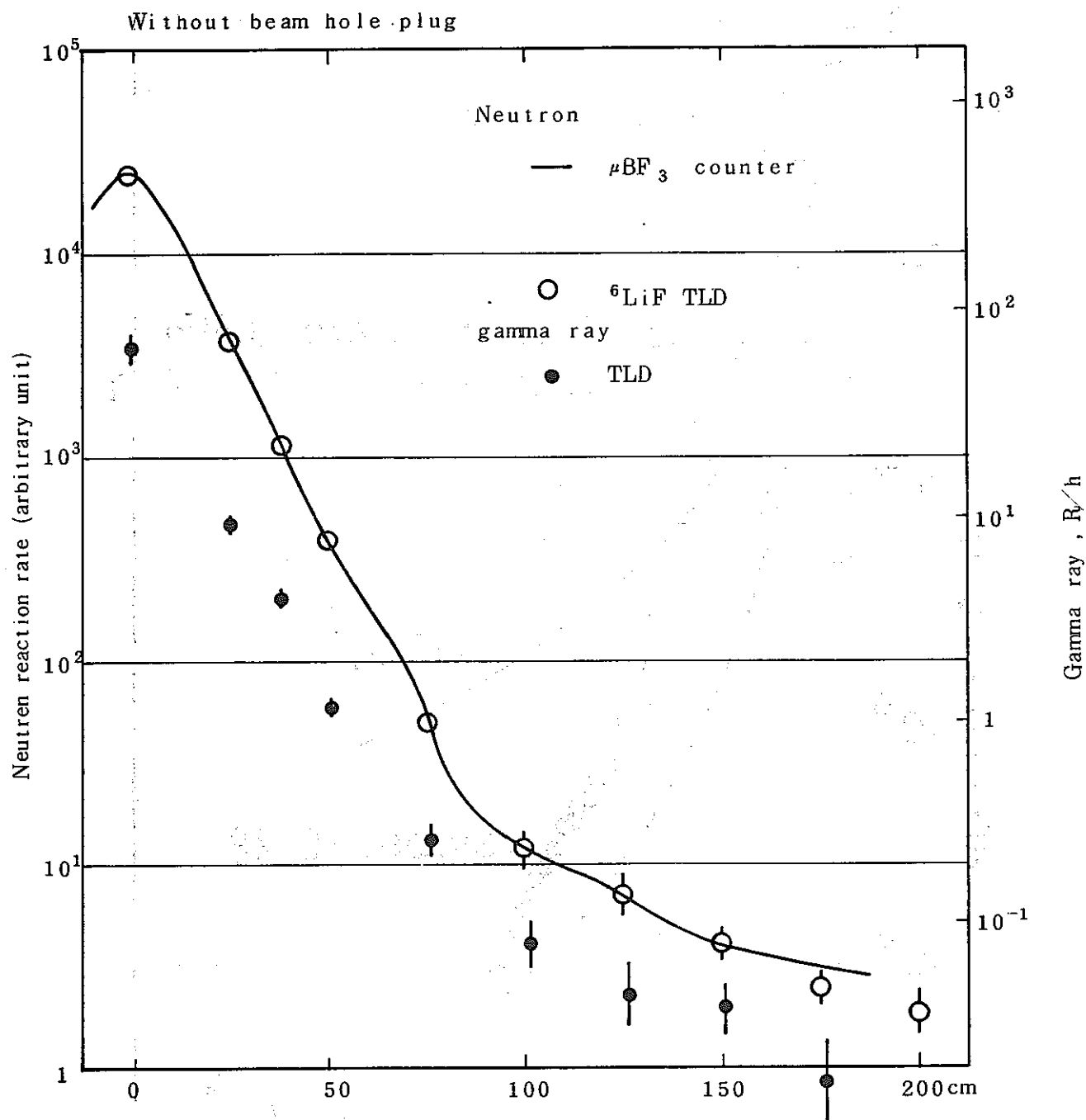


Fig. 4-42 Comparison among neutron reaction rate by  $^6\text{LiF}$  TLD, neutron counting rate by  $\mu\text{BF}_3$  counter, gamma-ray dose rate by TLD in No. 25 duct — "Without plug"

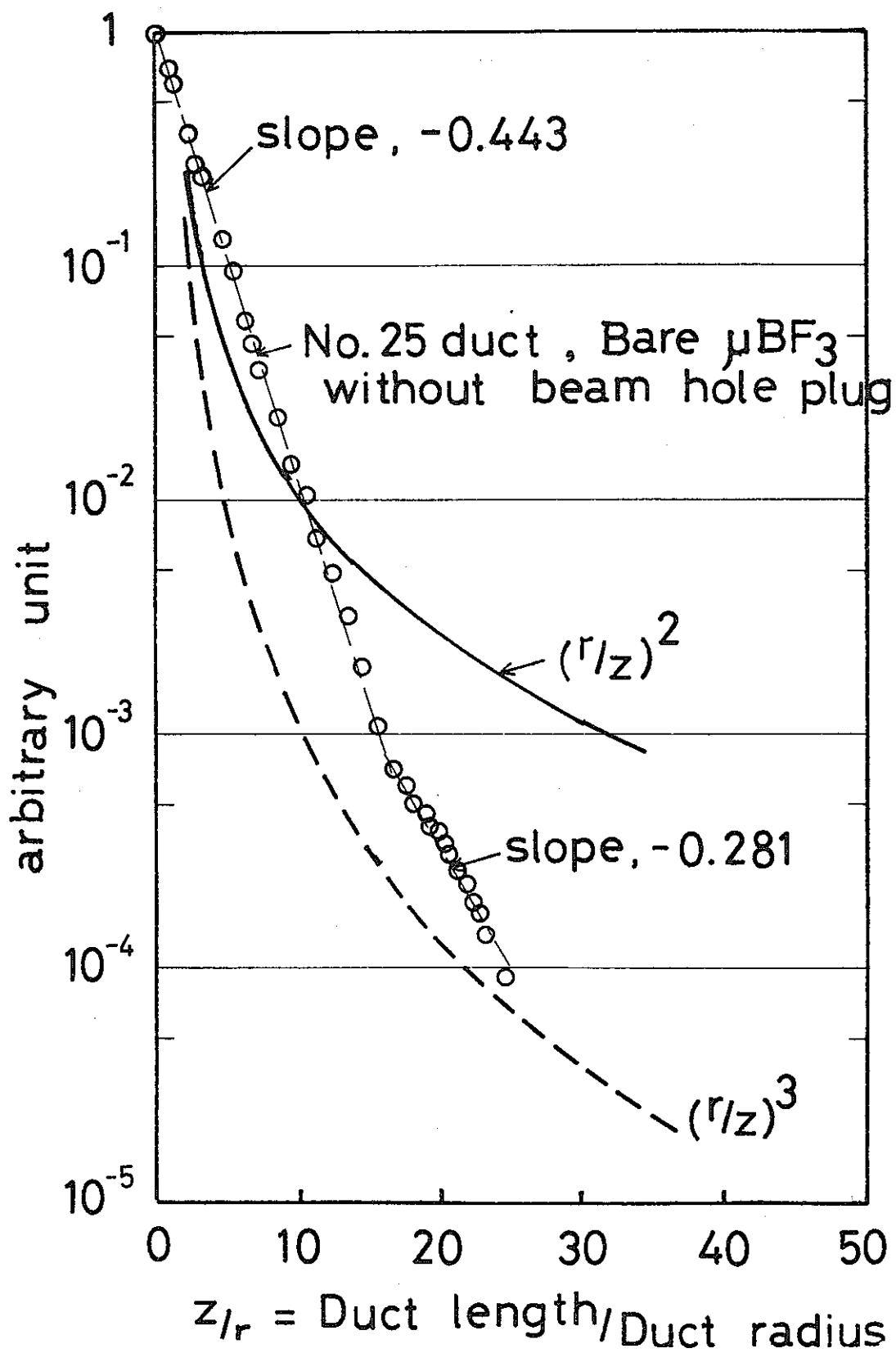


Fig. 5-1 Comparison between non-dimensional damping in No. 25 duct and analysis formula (Neutron counting rate by  $\mu\text{BF}_3$  counter — "Without plug")